AD A139 412 MICRO-REACTIONS OF METAL CONTACTS ON VARIOUS TYPES OF GAAS SURFACES(U) TECHNISCHE HOCHSCHULE DARMSTADT (GERMANY F R) INST FUER HOCHF.. H L HARTNAGEL ET AL. 1/1

UNCLASSIFIED JAN 84 DAJA45-83-C-0012 F/G 7/4 NL

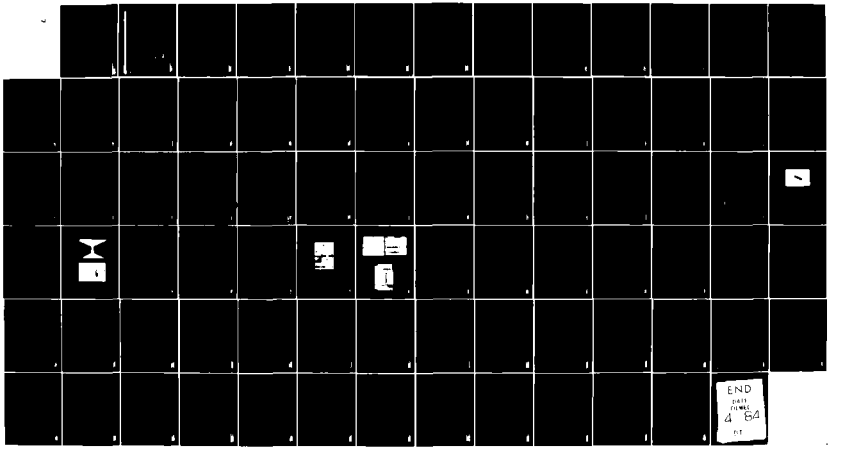

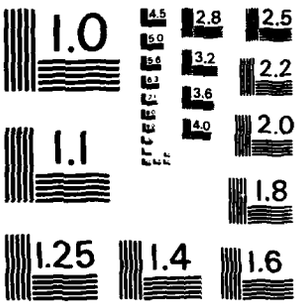

MICROCOPY RESOLUTION TEST CHART
NATIONAL BUREAU OF STANDARDS-1963-A

AD A139412

(11)

DTIC
ELECTE
MAR 2 7 1984
S D
A

Institut für Hochfrequenztechnik
Technische Hochschule
Darmstadt

This document has been approved for public release and sale; its distribution is unlimited.

DTIC FILE COPY

84 03 26 012

MICRO-REACTIONS OF METAL CONTACTS ON VARIOUS TYPES OF GaAs SURFACES

1st Annual Technical Report

H.L. Hartnagel[+]

E. Huber

K.H. Kretschmer

K. Röhkel

J. Würfl

JANUARY 1984

United States Army

EUROPEAN RESEARCH OFFICE OF THE U.S. ARMY

London England

GRANT NUMBER DAJA 45-83-C-0012

Technische Hochschule Darmstadt

Institut für Hochfrequenztechnik

Merckstraße 25, 6100 Darmstadt

G. F. R.

[+]Grant Holder

Approved for public release: distribution unlimited.

SECURITY CLASSIFICATION OF THIS PAGE (When Data Entered)

REPORT DOCUMENTATION PAGE

READ INSTRUCTIONS BEFORE COMPLETING FORM

1. REPORT NUMBER

2. GOVT ACCESSION NO. AD-A139 412

3. RECIPIENT'S CATALOG NUMBER

4. TITLE (and Subtitle)
Micro-Reactions on Metal Contacts on Various Types of GaAs Surfaces

5. TYPE OF REPORT & PERIOD COVERED
1st Annual Technical Report
January 1983 - January 1984

6. PERFORMING ORG. REPORT NUMBER

7. AUTHOR(s)
H.L. Hartnagel, E. Huber, K.-H. Kretschmer, K. Röhkel, J. Würfl

8. CONTRACT OR GRANT NUMBER(s)
DAJA 45-83-C-0012

9. PERFORMING ORGANIZATION NAME AND ADDRESS
Institut für Hochfrequenztechnik
Technische Hochschule Darmstadt
Merckstraße 25, 6100 Darmstadt, G.F.R.

10. PROGRAM ELEMENT, PROJECT, TASK AREA & WORK UNIT NUMBERS

11. CONTROLLING OFFICE NAME AND ADDRESS

12. REPORT DATE
January 1984

13. NUMBER OF PAGES

14. MONITORING AGENCY NAME & ADDRESS(if different from Controlling Office)

15. SECURITY CLASS. (of this report)

15a. DECLASSIFICATION/DOWNGRADING SCHEDULE

16. DISTRIBUTION STATEMENT (of this Report)

This document has been approved for public release and sale; its distribution is unlimited.

17. DISTRIBUTION STATEMENT (of the abstract entered in Block 20, if different from Report)

18. SUPPLEMENTARY NOTES

19. KEY WORDS (Continue on reverse side if necessary and identify by block number)
GaAs, Metallization Stability, XPS, ISS, GaAs surface chemistry

20. ABSTRACT (Continue on reverse side if necessary and identify by block number)
An XPS and ISS analysis of a range of GaAs surfaces is reported which are produced by various technological steps such as etching in basic or acidic solutions as costumary before the deposition of metals. Studies on the light emission for reverse biassed Schottky contacts has resulted in a better understanding of the influence of preevaporation etchants on this emission. First results of lateral material transport between co-planar electrodes and on Metal-GaAs interdiffusion due to typical operational device conditions are presented.

DD FORM 1 JAN 73 1473 EDITION OF 1 NOV 65 IS OBSOLETE

SECURITY CLASSIFICATION OF THIS PAGE (When Data Entered)

Table of Contents

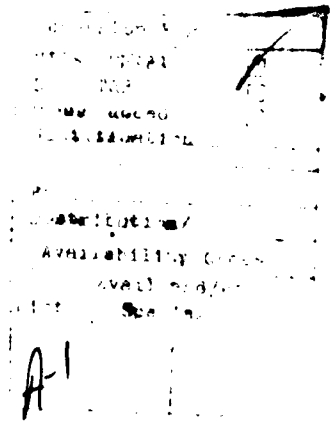

Abstract

An XPS and ISS analysis of a range of GaAs surfaces is reported which are produced by various technological steps such as etching in basic or acidic solutions as customary before the deposition of metals. Studies on the light emission for reverse-bias Schottky contacts has resulted in a better understanding of the influence of predeposition etchants on this emission. First results of lateral material transport between co-planar electrodes and across metal-GaAs junctions due to the application of high fields or currents are presented as to be found under operational conditions of devices such as MESFETs.

List of Keywords

GaAs, metallization stability, XPS, ISS, GaAs surface chemistry.

CHAPTER I

INTRODUCTION

GaAs-metal contacts are an important part of many microwave and optical devices, and the stability of these contacts is essential for the desired good life-times. It is necessary to consider such life-time effects in connection with realistic technology-type surfaces when the GaAs surfaces are not as ideal as produced by cleavage under ultrahigh vacuum. Such non-ideal GaAs surfaces can be expected to give strongly differing parameters for such life-time effects as field-assisted diffusion of metal along GaAs, or interdiffusion across the metal-semiconductor transition. The investigations described in this report therefore do not cover the phenomena associated with clean ideal surfaces. Indeed these have been the subject of intensive studies as found in numerous publications (for example see the Proceedings of the annual conferences on the Physics of Compound Semiconductor Interfaces, publ. regularly in J. Vac. Sci. Technol.). On the other hand, we do not study directly life-time effects on devices, as for example reported by various industrial laboratories (for example|1|).

We address our efforts towards a more fundamental study of the physics and chemistry of interactions associated with metals on GaAs surfaces as found with practical devices. Therefore firstly

an investigation is undertaken to evaluate the conditions of the GaAs surfaces as found after all the typical technology steps of device manufacture are applied such as sputter etching, rinsing in water, exposure to air, etching in common etchants etc. This has resulted in a large number of new, sometimes unexpected results relevant for an understanding of the various phenomena observed by device-fabrication technologists. In particular, this will be important to the second part of our program, namely the study of the stability of metal films on these GaAs surfaces under typical device-operational conditions such as high currents or high voltages. Here, interesting, new information can already be reported by us. However, more work is required to clarify all the related phenomena of device lifetime optimization.

A relatively simple test of the surface quality was proposed to be the amplitude of the light emission along the periphery of Schottky contacts [2] as particularly also seen with MESFETs (see for example [3]). The initial observations have now been substantiated and a physical understanding of the effects associated with this light emission has been derived.

CHAPTER II

Chemical XPS and ISS Study of Technological Surface Processing Steps Usually Applied Before Metallization

Previous results gave an indication that the light emission intensity from the periphery of the reverse biased GaAs-Schottky-barrier diodes depends on the chemical surface treatment of the GaAs samples prior to Schottky metal deposition. Samples etched in NaOH + H_2O_2 (1/1 mixture of 2 % p. weight NaOH and 1.2 % p. volume H_2O_2) or other alkali solutions give good light emitters. Samples etched in concentrated HCl or other strong acids, however, do not emit any light or show only weak emission. The spectral distribution of this emission is not affected by the etchant. Adachi and Hartnagel[4] suggested that the light emission intensity is influenced by the surface conditions of the samples, which might be different for different surface treatments.

Such surface conditions would certainly have a profound influence on the stability of the metal-semiconductor system. It is therefore valuable to systematically assess the chemical and physical conditions of the GaAs surface before any metal film is deposited. Therefore, an XPS and ISS analysis of GaAs surfaces was undertaken after applying a variety of technology-etchants. XPS gives useful information on the chemical bonding of such surface atoms, whereas ISS yields information only about the top surface monolayer. By using the 2p and 3d lines of XPS, information at two

different depths can be obtained. In Fig. 1 the XPS spectra resulting from the As $2p_{3/2}$, As 3d, Ga $2p_{3/2}$, Ga 3d and O 1s core levels are given. The $2p_{3/2}$ level peaks of As and Ga are more surface sensitive than the 3d level peaks. Therefore, a change in surface stoichiometry will first appear in the $2p_{3/2}$ peaks.

The rows in Fig. 1 indidate the different surface treatments applied:

row 1 etched in NaOH + H_2O_2

row 2 etched in concentrated HCl after etching in NaOH + H_2O_2

row 3 sputtering with 3 keV ions in the XPS facility

row 4 etched in HCl after sputtering

row 5 etched in NaOH + H_2O_2 after sputtering

row 6 1 day stored in air after sputtering

row 7 1 day stored in air after etching in NaOH + H_2O_2

In the first column the As $2p_{3/2}$ XPS peaks are given. One can resolve two peaks caused by a chemical shift. The peak at lower binding energies is due to As bonded in GaAs or elemental As, while the peak shifted to higher binding energies represents an oxidised state of As. The oxidised As peak is always present in the NaOH + H_2O_2 etched samples (rows 1,5) or in samples stored in air (rows 6,7). However, the peak is not present or only weakly present in the HCl etched (rows 2,4) and sputtered samples (row 3). After sputtering the highest As $2p_{3/2}$ peaks appear because of the clean surface. Storage in air gives the lowest peak heights due to a thicker nativer oxide layer.

A second column shows the As 3d peaks. These peaks reflect the more bulk-like composition of the surface, which is scarcely influenced by the different surface treatments. The large peaks of non-oxidised As dominate the figures, oxidised As can be seen only weakly in the NaOH + H_2O_2 etched (rows 1,5) and in the air stored samples (rows 6,7).

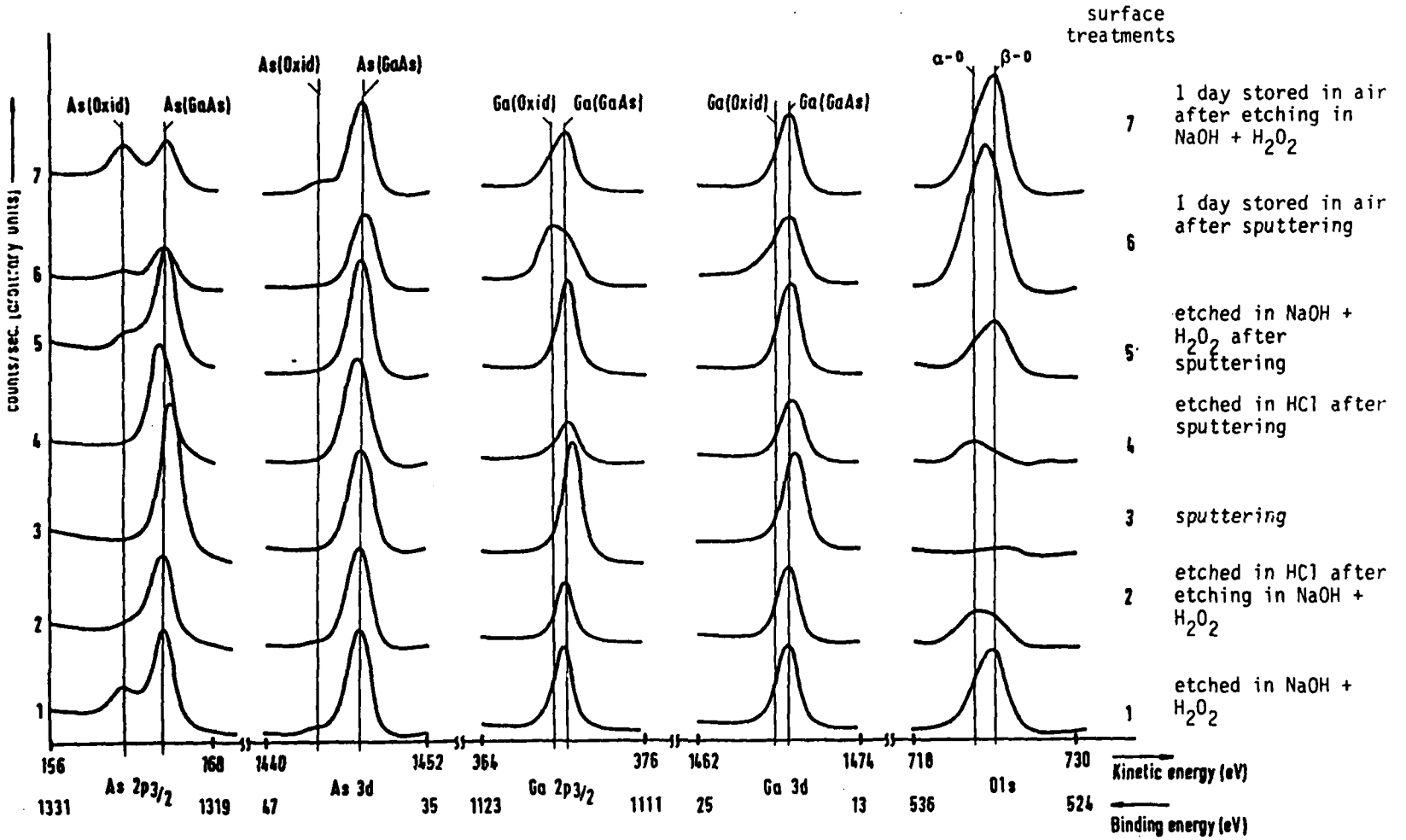

Fig. 1

XPS-spectra of GaAs(100) surfaces after different surface treatments
The As $2p_{3/2}$ As 3d, Ga $2p_{3/2}$, Ga 3d and O 1s core level peaks are shown

In the third column the Ga 2 $p_{3/2}$ peaks are given. It is striking that only the air stored samples (rows 6,7) and the HCl etched sample with a sputtered starting surface (row 4) show the chemically shifted GaAs peaks which indicate oxidised Ga. No oxidised Ga is present on NaOH + H_2O_2 etched surfaces (rows 1,5). HCl seems to dissolve Ga because the Ga to As peak height ratio is lower in HCl etched samples (rows 2,4) tha[illegible]th other surface treatments. In curves obtained with a sputter[illegible]tarting surface (rows 4,6) the damage introduced by sputteri[illegible] is obvious because of the larger amount of dissolved Ga in the H[illegible]etched sample and the larger amount of oxidised Ga in the air stored sample compared to the starting surface etched in NaOH + H_2O_2.

The Ga 3d peaks in the fourth column reflect the changes introduced by surface treatments more weakly than the surface sensitive 2 $p_{3/2}$ peaks.

In the fifth column the O1s peaks are given. HCl etched samples (rows 2,4) show a lower amount of O compared to NaOH + H_2O_2 etched samples (rows 1,5), while the sputtered surface (row 3) shows nearly no oxygen. The chemical shift of the O1s peak obtained with HCl and H_2O_2 etched samples indicates two different bonding states of oxygen. A similar chemical shift of the O1s levels was obtained by Ranke et al[5] on GaAs surfaces prepared by ion bombardment and annealing. The ratio of oxygen with higher 1s binding energy (α-oxygen) to oxygen with lower 1s binding energy (β-oxygen) was nearly idependent of the surface orientation.

This suggests a connection between the formation of α- and that of β-oxygen. β-oxygen, which causes a chemical shift of the Ga 3d XPS peaks in contrast to α-oxygen is therefore attributed to oxygen directly bonded to Ga.

The chemical state of α-oxygen is still in doubt, however, a model was proposed that defects created by the formation of the Ga-O bonds serve as adsorption sites for α-oxygen.

In our experiment a strong dependence of the α-oxygen- to β-oxygen-concentration ratio on the chemical surface treatment was found. The sample etched in NaOH + H_2O_2 (row 1) shows only the β-oxygen emission peak, which is attributed to oxygen bonded to As as indicated by the simultaneous chemical shift of the As 2 $p_{3/2}$ peak. At the sample surface etched in HCl (rows 2,4) a considerable amount of oxygen is bonded in the form of α-oxygen. This is also confirmed by the small amount of chemically shifted Ga and As.

The samples stored in air (rows 6,7) show a mixture of both α- and β-oxygen. The sample pretreated by sputtering (row 6), however, shows a larger amount of α-oxygen than the NaOH + H_2O_2 pretreated sample (row 7), which might be due to the additional amount of defects acting as adsorption sites introduced by sputtering.

By ordering the sample treatments according to the amount of α-oxygen present it is striking that the amount of chemically shifted Ga obtained from the Ga 2 $p_{3/2}$ peak heights follows the same scheme. This confirms the connection between the chemisorption of α-oxygen and the formation of the Ga - O bonds only. Indeed it can be seen from Fig. 1 that the existence of As - O bonding is not relevant for the occurance of α-oxide.

All curves obtained with the sputtered surface (row 3) show a shift of the XPS-peaks to lower binding energies. This uniform shift of all lines indicates a different surface potential of the electron-emitting sample surface. This might be caused by the damage introduced by sputtering.

From the measurements the following conclusions on surface composition concerning the NaOH + H_2O_2 (bright light emission) and HCl (weak light emission) etched samples can be drawn.

NaOH + H_2O_2 : O is only bonded to As, not to Ga
A nearly stoichiometric conentration ratio exists between As and Ga

HCl : O that was bonded to As, that is the native oxide, is removed
O is only bonded to defects at the surface.
The Ga to As concentration ratio is less than 1

The results presented so far concern the etch NaOH + H_2O_2 which removes GaAs layers by a reaction limited etch rate. These measurements are extended then to investigate the chemical composition of GaAs surfaces after application of a diffusion limited etch. Therefore, bromine-methanol was chosen as a suitable etch, which gives a mirrow-like finish to the GaAs surfaces as is typical for a diffusion limited etchant.

Fig. 2 shows the Ga $2p_{3/2}$, As $2p_{3/2}$ and O 1s XPS peaks of GaAs-surfaces treated in different etches. In the first row (always counted from the bottom), the sample was etched in bromine-methanol (5 vol.-% Br in CH_3OH) for 15 seconds and afterwards rinsed in methanol. The second row shows a sample also etched in bromine-methanol and rinsed in H_2O. In the third row the XPS results of a sample etched in NaOH + H_2O_2 (1/1 mixture of 2 % per weight NaOH and 1,2 % per vol. H_2O_2 in H_2O) and rinsed in H_2O is given. The fourth row shows the XPS results of a sample etched in NaOH + H_2O_2 and rinsed in methanol.

In the first column, the As $2p_{3/2}$ XPS peaks are given. The second and third columns show the Ga $2p_{3/2}$ and O 1s XPS peaks respectively.

The sample etched in bromine-methanol and rinsed in CH_3OH (row 1) show only a small amount of oxidised As in the form of As_2O_3. No As_2O_5 is present. The amount of oxidised Ga is also negligeable. The oxygen peak consists of two interfering peaks of β-oxygen bonded in As_2O_3 and α-oxygen chemisorbed to defects at the GaAs surface.

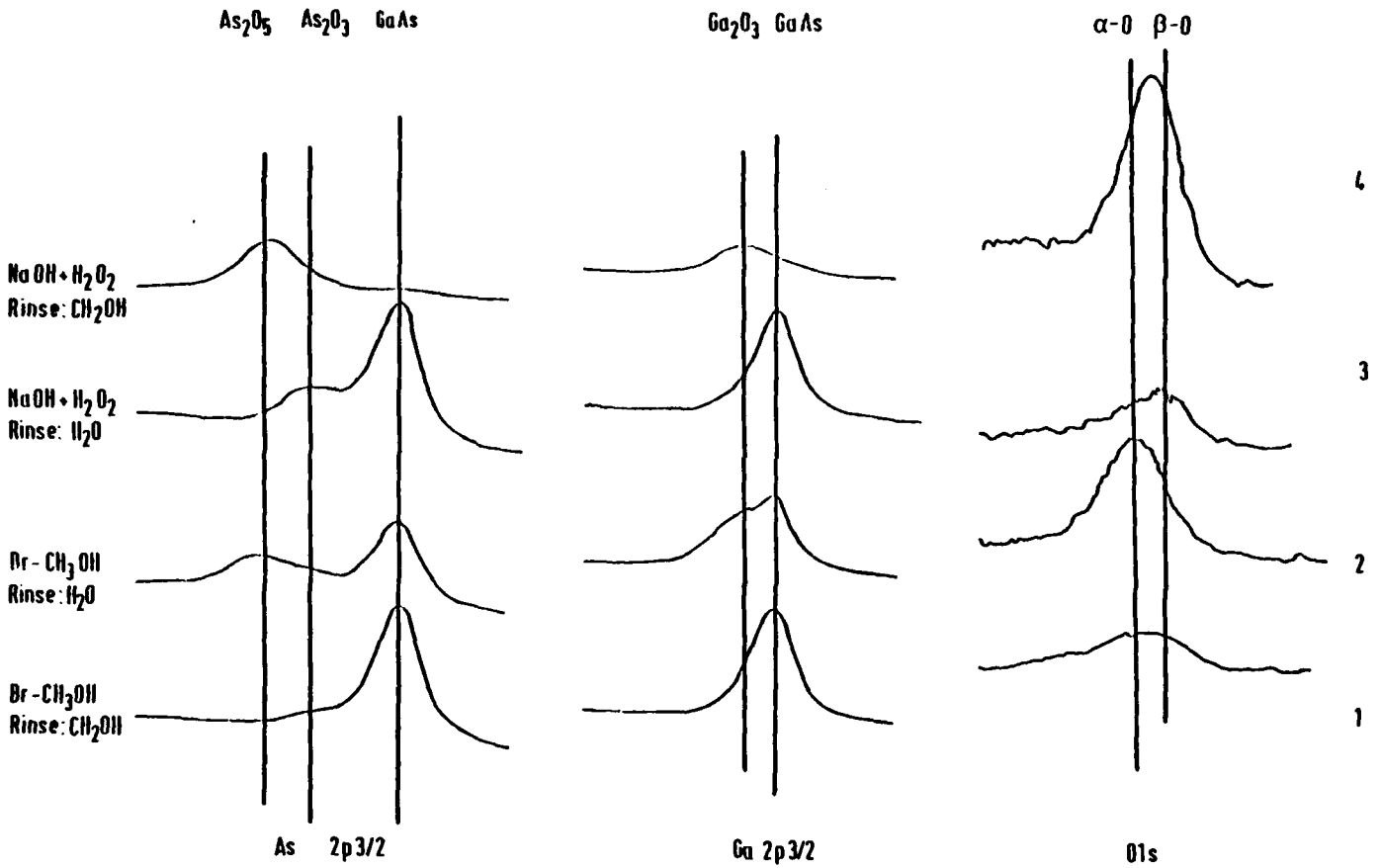

Fig. 2 XPS-spectra of GaAs(100) surface etching with NaOH + H_2O_2 or Br-CH_3OH and subsequent rinsing in CH_2OH or H_2O

Rinsing the bromine-methanol etched sample in deionised water (row 2), however, gives a strongly oxidised surface. The oxide consists mainly of As_2O_5 and Ga_2O_3. A smaller amount of As_2O_3 is also present. The oxygen peak shows a large amount of chemisorbed α-oxygen.

For comparison, the XPS-spectrum of a sample etched in NaOH + H_2O_2 as given already in Fig. 1 above is shown in the third row. There the surface is covered mainly by As_2O_3. No As_2O_5 and practically no Ga_2O_3 is present. Oxygen is bonded mainly in the form of β-oxygen. In the forth row the XPS results of a sample etched in NaOH + H_2O_2 and rinsed in methanol is given. The surfaces consist of a large amount of As_2O_5 and Ga_2O_3. This oxide is thick enough to nearly prevent photoelectrons from the bulk GaAs.

From the measurements, the following conclusion can be drawn. The bromine-methanol etch with rinse in methanol gives no oxidised Ga or As at the GaAs surface. Bromides, which may remain on the GaAs after the etch, are dissolved by the methanol rinse. The bromine-methanol etch with rinse in water, however, gives a totally different result. Now the surfaces are strongly oxidised. Gallium oxide and two oxides of As are present at the surfaces. The mechanism for this rapid oxidation might possibly include an oxidation of gallium or arsenic bromide.

The mechanism of the NaOH + H_2O_2 etch is different from that of bromine-methanol. H_2O_2 is an oxidising agent, which leads to the production of a surface oxide. This oxide, however, is then dissolved by the NaOH solution. If the sample is rinsed in methanol after etching in NaOH + H_2O_2, the actual surface is conserved. It shows a thick layer of Ga_2O_3 and As_2O_5. By rinsing the NaOH + H_2O_2 etched surface in deionised water, the oxides are dissolved. The remaining surfaces shows no oxidised Ga. However, oxidised As is present, but in this case in the form of As_2O_3.

The above results show clearly that the NaOH + H_2O_2 etch should not be used if minimisation of oxygen is wanted. Using the bromine-methanol etch, the use of H_2O for rinsing the sample should be avoided.

Now a study is presented on native air-exposed GaAs-surface composition and the sputter-cleaning transient. These results are based on both XPS and ISS.

As outlined above, a device manufacturing based on single-crystal thin-film epitaxy, metal and insulator deposition and other processes, uses air exposed polished and organic-solvent cleaned (100)-GaAs surfaces. These are often cleaned by sputter etching several surface-layers away. Therefore an additional study was undertaken to obtain still further information on the original compositions of such surfaces and on the sequence of material removal by sputtering. The measurements weren undertaken by ISS (Ion Scattering Spectroscopy) to analyze the very surface layer and by the XPS system described above.The reader is reminded here that in connection with the latter facility the emission depth ranges from around 5 - 8 Å for the $2p_{3/2}$-orbitals to around 20 - 30 Å for the 3d-orbitals of Ga- and As-atoms.

The (100)n-GaAs sample was grown bulk material doped with a carrier density of 10^{16} cm^{-3} and delivered sliced and polished by the manufacturer Wacker. It had been stored in air for a long period of time. After organic-solvent cleaned in trichlorethylene, acetone and methanol, the samples were mounted on a steel support using conducting silver paint and inserted into the ultrahigh vacuum system of the measurement facility of < 10^{-9} mbar. To obtain ISS-signals ions of ^{4}He and ^{20}Ne with a primary energy of 1000 eV were used. The angle of elastic scattering was fixed to 134 degree. XPS was undertaken with an Al-$K\alpha_{1,2}$ X-ray emitting

anode with a line of about 1 eV FHWM. Ion etching was done by Ne^+- and Ar^+-ions.

The XPS-spectra are shown in Fig. 3 starting with the lowest row, denoted by 1, with the unsputtered original surface of the GaAs-sample. The following rows up to row 5 show the XPS-spectra after the surface was bombarded with Ne^+-ions. The highest row 6 shows the spectra after the surface had been etched for nearly half an hour with Ar^+ of 3000 eV accelerating potential.

At the initial surface (row 1) a large amount of As_2O_3 and Ga_2O_3 is to be seen where the As_2O_3 occurs, however, only within a thin layer zone, because after a first Ne^+ etching, the oxide signal vanishes from the more bulk-sensitive As-3d peak (rows 2,3), and is only still detectable within the more surface-sensitive As-$2p_{3/2}$ peak (rows 2,3). Ga_2O_3 is much more deeply burried in the GaAs sample as is to be seen from the peaks of Ga-$2p_{3/2}$ and -3d (rows 4,5). Whereas no As_2O_3 is detectable up to row 4 there still remains a Ga_2O_3 part in the Ga-orbitals and now a symmetrical O 1s peak occurs.

From the O 1s spectra it is to be seen that the As_2O_3 results in a broadening of the O 1s-peak to higher kinetic energies (i.e. smaller binding energy), which is more pronounced as can be recognized from Fig. 4 which shows the spectra of the same sample after having been released to air for nearly 30 min (row 2). The spectra of row 1 represent the data after the last heavy Ar^+ etch. A

subsequent first ion-etch (or, what yields the same outcome, namely heating the sample surface by radiation of a filament up to 150° - 200° C) takes away all As_2O_3 as to be seen from the As 2p peak (Fig. 2, row 3) and reduces the broadened oxygen O 1s peak (i.e. two peaks originally overlapping, row 2) into a symmetrical one (row 3) related now solely to Ga_2O_3.

Comparing the initial spectra (Fig. 3, row 1) with those after the last ion-etch with Ar^+ (row 6) there follows a singnificant shift of about nearly 1 eV for all of the peaks as is indicated in Fig. 3 for the case of the As $2p_{3/2}$- and As 3d-orbitals. The shift mainly occurs after the initial As_2O_3 has vanished when Ga_2O_3 solely remains in the GaAs surface. The subsequent etching causes then significant peak-shifts (see Fig. 3, row 4 upwards).

It is likely that this represents a reduction in surface potential starting with etching the Ga_2O_3-zone. Re-oxidizing the etched sample for a short time in air results in a nearly reversible 1 eV shift-back of all peaks (Fig. 4, rows 2,3) to the original energy positions which had been taken before etching away the last remaining Ga_2O_3-zone (Fig. 3, rows 2,3). A new heavy Ar^+ etch (etching of Ga_2O_3-zone) again results in a nearly 1 eV shift of all the peaks (Fig. 4, row 4) indicating a surface potential reduction as was described before.

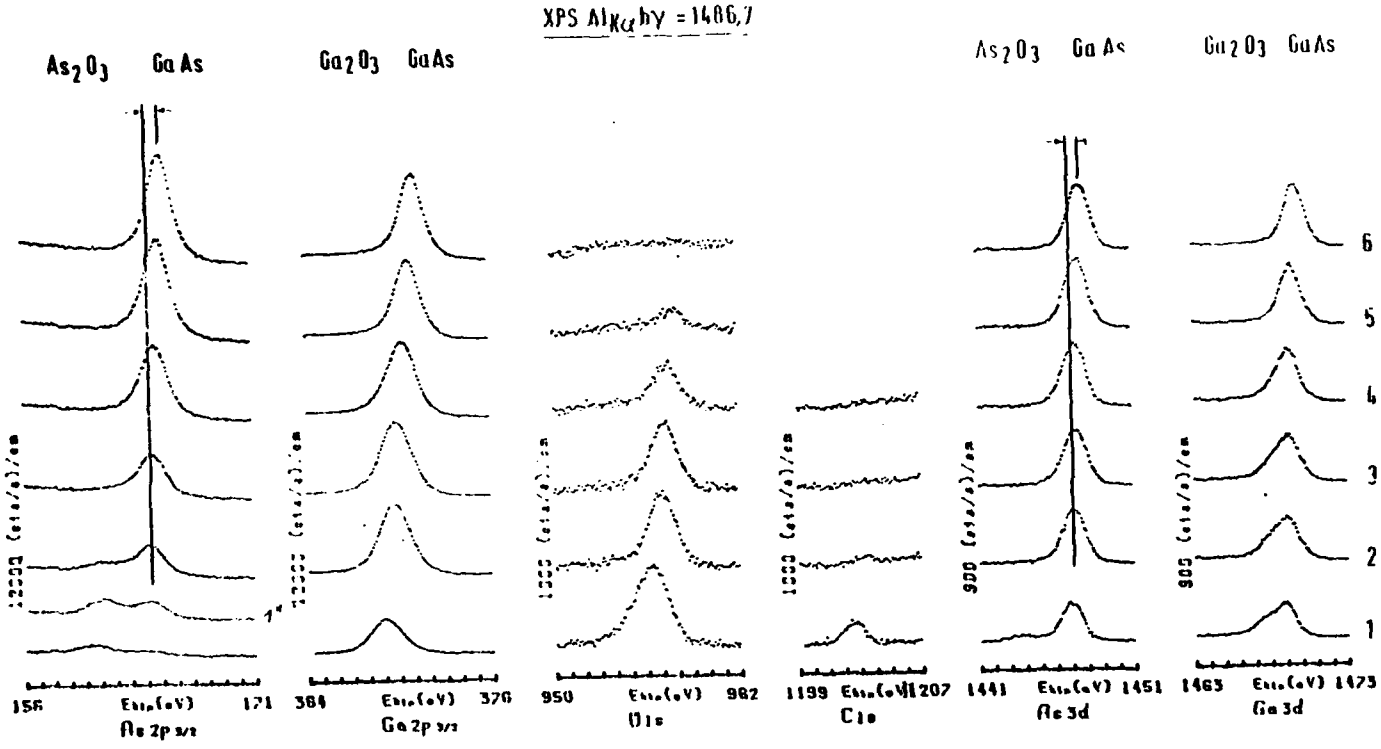

Fig. 3 XPS-spectra

row 1 original GaAs-sample as inserted into the vacuum system

row 2 to 5 subsequent etching with Ne^+ of different intensities and duration

row 6 last etch step when Ar^+ was used (Ar^+ is much heavier than Ne^+)

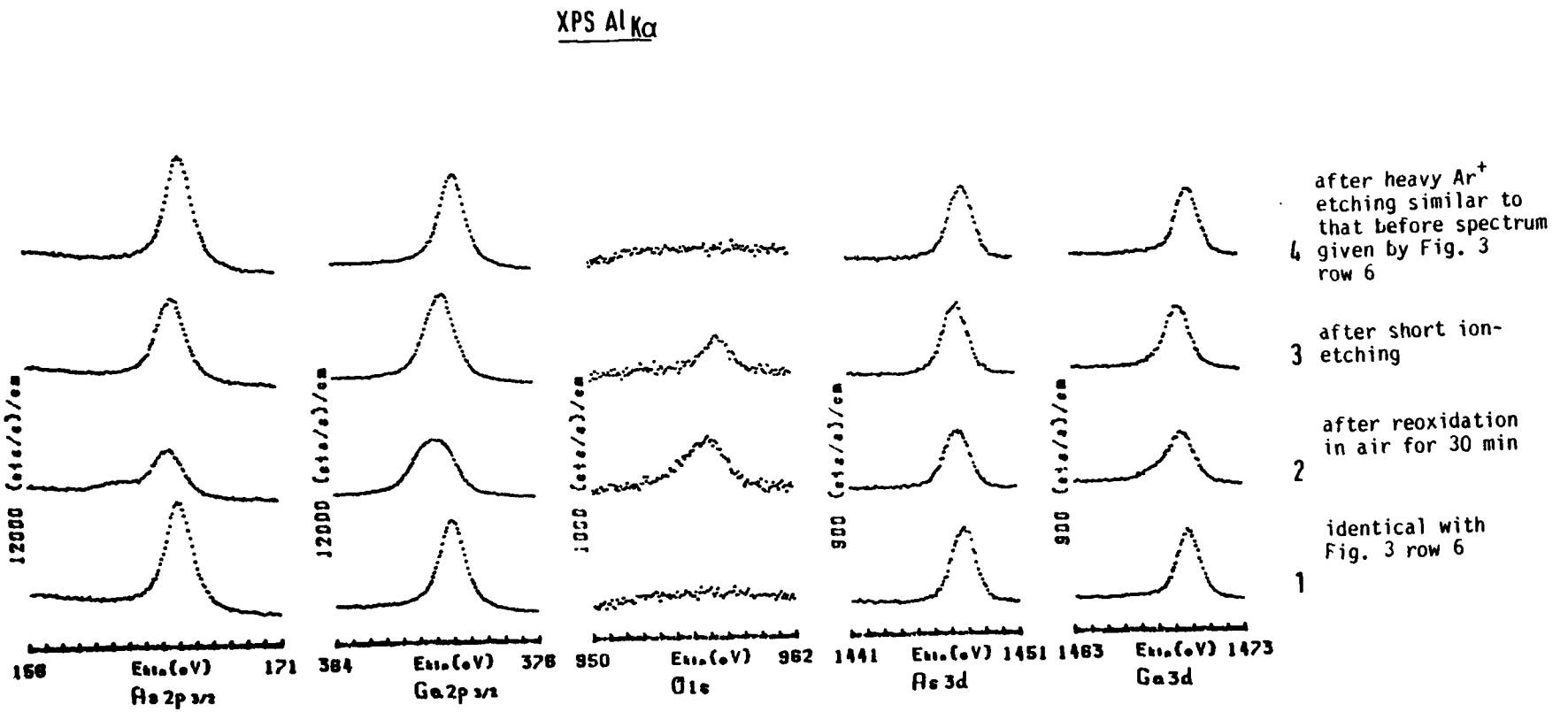

Fig. 4
XPS-spectra

Further it can be seen that the original unsputtered surface (Fig. 3, row 1) firstly is covered by an extremely thin adsorption-layer (probably a mixture of water film, and a carbon-hydrogen-oxide film), the resulting contamination of having air-exposed the sample for a long period of time. The prominent C_1-signal strongly diminishes after the first etch. That contamination itself is easily removed by only bombarding the surface with the comparatively light He^+-ions of 1000 eV energy as used for ISS analysis. The resulting XPS-spectrum of the surface sensitive As $2p_{3/2}$ orbital (Fig. 3, row 1*) shows after the bombardement a nearly unaltered ratio of As_2O_3 to As|GaAs| but a more intensive signal. Because of the extremely short free wave length of the As $2p_{3/2}$ core-electrans even monolayers contaminating the sample-surface results in a strongly reduced signal height. Also the ISS analysis by elastically scattering ^4He leads to the same conclusions of a first monolayer of contamination.

Fig. 6 shows a typical ISS-spectrum in the this case related to the XPS-spectrum after reoxidizing the surface for a short time (Fig. 4, row 2). Comparing this ISS-spectrum with that taken just after having inserted the sample into the vacuum system (Fig. 7, row 1) the following can be found: an extremely reduced signal intensity of Ga and As (which are overlapping each other in the case of ^4He), nearly no oxygen, and a more pronounced noisy background can be seen thus indicating a contamination over layer on top of the sample-surface.

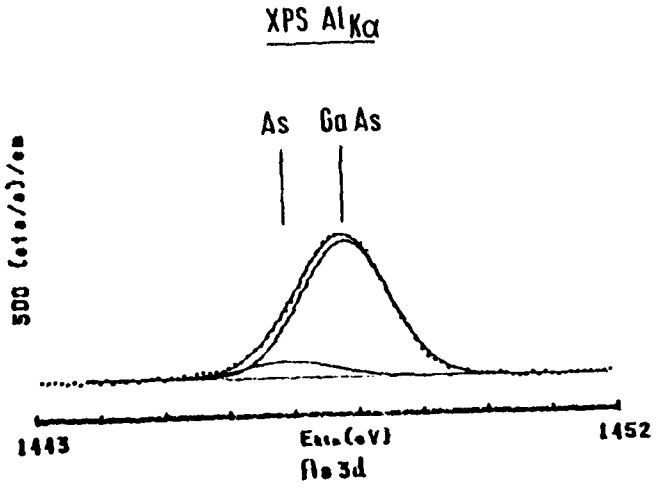

Fig. 5

Curve-fitted experimental spectrum of the As 3d - orbital of Fig. 3 row 6

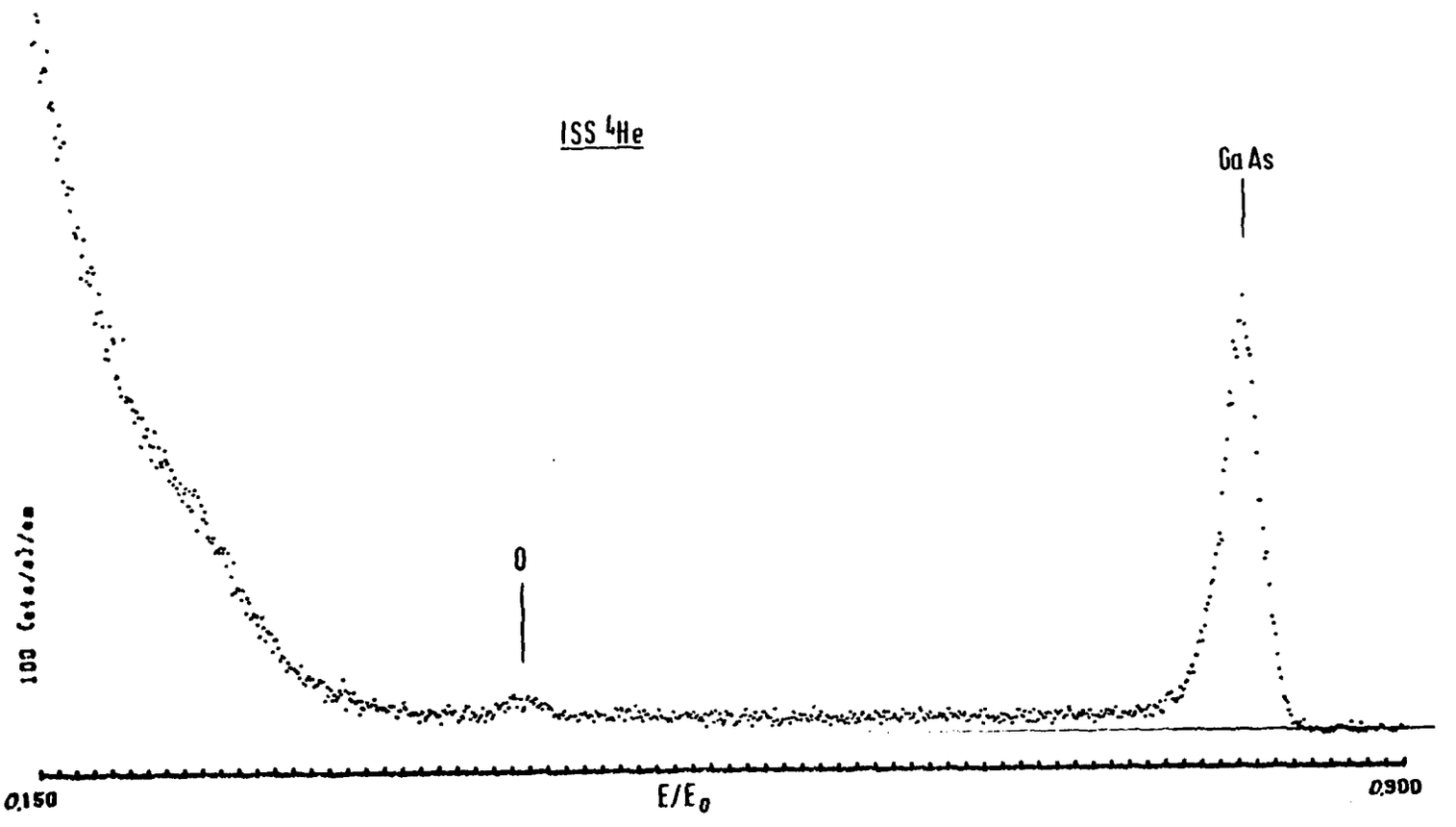

Fig. 6

^{4}He-ISS aquivalent to XPS of Fig. 4 row 2

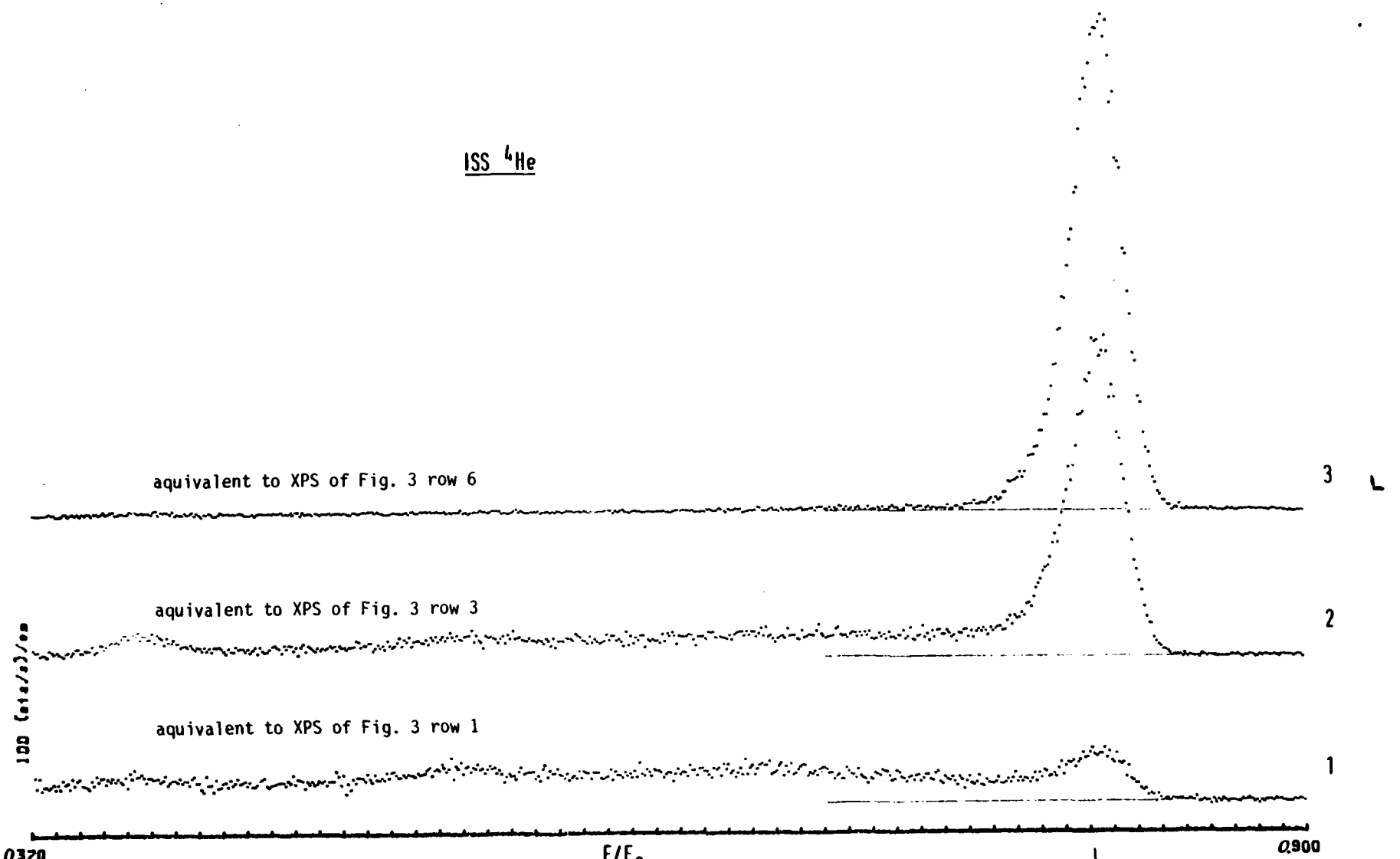

Fig. 7
^{4}He-ISS spectra

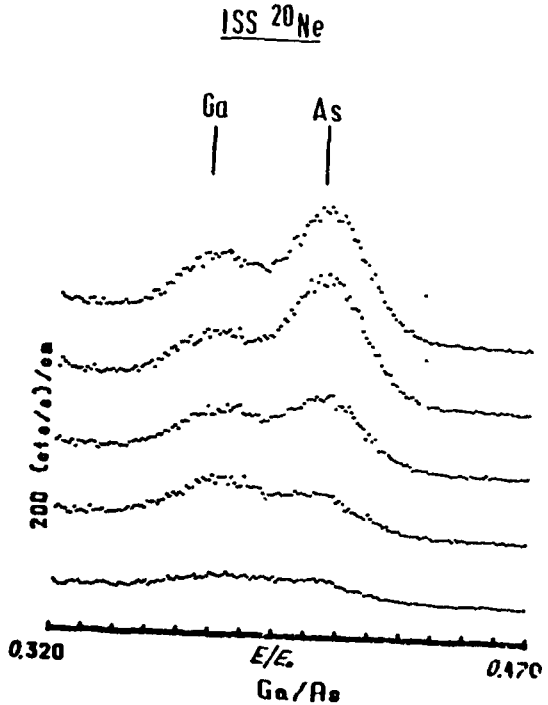

6 aquivalent to XPS of Fig. 3 row 6

5 aquivalent to XPS of Fig. 3 row 5

4 aquivalent to XPS of Fig. 3 row 4

3 aquivalent to XPS of Fig. 3 row 3

2 aquivalent to XPS of Fig. 3 row 2

Fig. 8

^{20}Ne-ISS spectra

A remarkable effect of sputter-clearing is the accumulation of pure arsenic in the sample-surface. Fig. 5 shows the more detailed XPS-spectrum of Fig. 3, row 6 of the As 3d-orbital taken after the last heavy Ar^+-bombardement. Because the background is linear and very small the experimental XPS-signal could be simply fitted by two Lorentz-Gauß lines seperated by 0,9 eV, just the difference of binding energy for pure As and GaAs-bounded arsenic.

The ISS (^4He) spectra of Fig. 7 indicate a reduction of noise and background intensity for further sputter-cleaning of the sample surface. A direct comparison of the O-reduction with the Ga/As increase, to obtain possible information of knocking-on effects of O due to sputter-clearing, therefore remains problematic and was not undertaken.

The elastic scattering of the havier ^{20}Ne-ions of the sample surface enables one to distinguish between ions scattered by Ga-atoms and those scattered by As-atoms (Fig. 8), whereas oxygen, because its mass is smaller than the used ^{20}Ne ion, cannot be detected anymore. The ISS-spectrum of Fig. 8, row 6 is taken from the heavy Ar^+ etched sample surface related to the XPS-spectra of Fig. 3, row 6. Because the oxidized zones are sputtered away the stoichiometry of Ga to As is expected to be 1 : 1. Because Ga consists of the two stable isotopes ^{69}Ga and ^{71}Ga whereas As consists only of ^{75}As, the peak of Ga is lower and broader than that of As. From Fig. 8 it can be seen that during sputter-cleaning significant changes of Ga to As ratios occurs. From more detailed ^{20}Ne-ISS measurements a

relative depth-profile concerning the Ga to As ratios could be obtained (Fig. 9). The calibration in depth of the subsequent etch steps is only vague, because the selected changes of current densities and accelerating energies during sputtering can not be related exactly to the actual etch rates obtained. But from a comparison with the simultaneously performed XPS measurements the following results, shown in Fig. 9, can be found: at the initial surface and as long as there is As_2O_3 to be seen from the XPS-analysis there exists a Ga-enriched phase. After having sputtered away all As_2O_3 (compose Fig. 3, row 4 upwards) a change of the Ga : As ratio takes place. Up to the etch-step where oxygen (and thus Ga_2O_3) is no more detectable, an arsenic-enriched phase of the sample occurs.

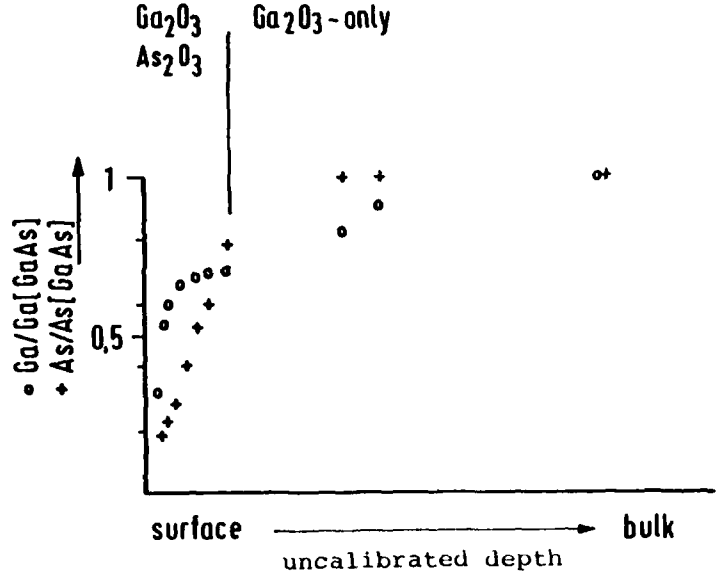

Fig. 9

Depth profile of Ga and As by detailed ^{20}Ne-ISS analysis

Ga|GaAs| : concentration of Ga in GaAs-compound
As|GaAs| : concentration of As in GaAs-compound
Ga : concentration of Ga after the given etch step
As : concentration of As after the given etch step

CHAPTER III

The Etch Effects on Light Emission

Simultaneously the variation in light intensity with the etchant, there is also a variation in the current voltage (I-V) characteristics. Fig.10 shows the I-V-characteristic of 3 Schottky barrier diodes of different doping concentration etched in NaOH + H_2O_2. There are two different conduction mechanisms visible in Fig. 10. At low voltages, the current is due to the tunneling effect (field emission or thermonic field emission). At higher voltages, eventually another conduction mechanism, the avalanche breakdown, dominates. Only in the 10^{18} cm^{-3} doped sample, the tunneling current component is so large that avalanche breakdown can not be attained. The voltage at which avalanche breakdown starts to outweigh the tunneling effect is about 11 V in the 2 . 10^{16} cm^{-3} doped sample and about 3.5 V in the 4.8 . 10^{17} cm^{-3} doped sample. The avalanche breakdown leads to the so-called hard reverse I-V characteristic with a positive temperature coefficient of breakdown voltage. The tunneling breakdown, however, gives a soft reverse characteristic with a negative temperature coefficient. Only samples with avalanche breakdown show light emission.

If the HCl etchant is applied to the samples, the breakdwon voltage is generally reduced. However, from the temperature dependence and the shape of the I-V characteristics, two different mechanisms for non light emitting diodes can be distinguished.

Samples of lower doping concentration show still a hard reverse characteristic like the NaOH + H_2O_2 etched samples and a positive temperature coefficient, which indicates avalanche breakdown. Samples of higher doping concentration (> 2 . 10^{17} cm^{-3}), however, often show the soft characteristic and a negative temperature coefficient of tunneling breakdown.

With the results obtained by I-V and XPS measurements, one can explain the influence of the HCl etchant on light emission in the following two ways:

1. The depletion of Ga in the near - surface region increases the effective doping concentration, because Ga defects act as deep donors. This leads to an increased surface field strength and therefore to an increased tunneling component in the current. The avalanche component, however, which is responsible for light emission, is reduced appropriately.

2. The HCl etchant reduces the thickness of the native oxide layer and creates defects at the surface. At the defects below the contact area, a localised avalanche with a reduced breakdown voltage may take place. The voltage for breakdown at the periphery of the contact pad is therefore not attained. Light emission from the localised spots, however, may be hidden by the contact pad.

The results show that the effect of surface treatment on light emission is not a primary effect, which influences the light emission itself. It rather seems to be a secondary effect, which influences the light emission by the changes in the current conducting properties.

CHAPTER IV

Metal Instability on GaAs Surfaces

A substantial contribution to the failures of GaAs devices represents the metal instability[1,6]. This can be divided into the following three effects:

1. material transport between electrodes along the GaAs surface upon the application of high fields (see also for example [7]); here many additional effects can occur such as the initial sputtering of material by the bombardment from ionizing field breakdown in the atmosphere immediately above the electrodes;

2. interdiffusion of material across the metal-semiconductor interface due to the application of high currents or fields; and

3. electromigration along narrow conductors with extremely high current desities, due to the so-called electron wind.

Here, so far, the first two types of effects have been studied whereas the third type will receive our attention next year, when an additional research fellow will join us.

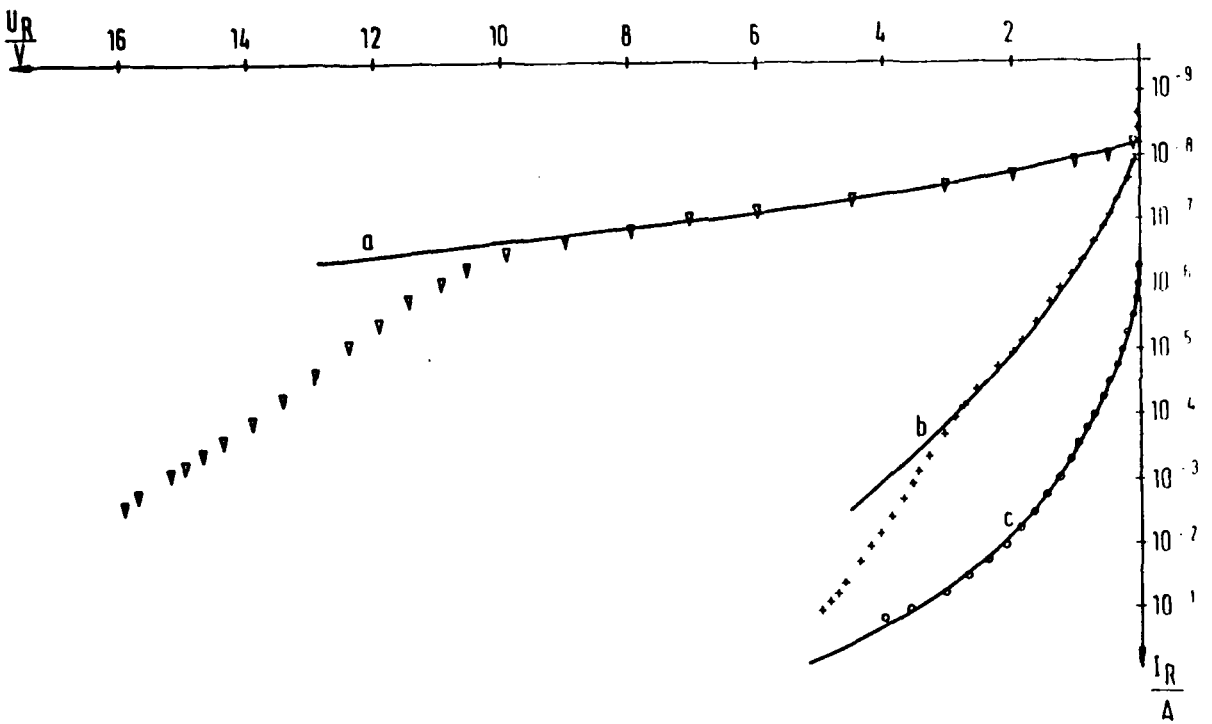

Fig. 10 Reverse I-V characteristics of GaAs Schottky barrier diodes of different doping concentrations (a) $n = 2 . 10^{16}$ cm^{-3}; (b) $n = 4.7 . 10^{17}$ cm^{-3}; (c) $n = 1 . 10^{18}$ cm^{-3}

The solid lines are calculated tunneling currents for the following doping concentrations (a) $n = 2 . 10^{16}$cm^{-3}; (b) $n = 3.5 . 10^{17}$ cm^{-3}; (c) $n = 1.5 . 10^{18}$ cm^{-3}

IV.1 Basic Concepts of Material Transport

All the 3 effects outlined above of material transport can be associated with a periodic potential function forming potential troughs where either atoms rest or where they can move into, due to the combined effort of thermal vibrations and the additional forces of electric fields or an electron wind. The approximate material flow equation for phenomena in solids is given by [8]

$$J = C_1 \quad \rho_e j \cdot \frac{N}{kT} D_o \exp\left(\frac{-Q}{kT}\right) \ldots \qquad (1)$$

with ρ_e - the resistance of vacancy flow

j - the electric current density

N - the defect density

D_o - the diffusion coefficient

Q - the activation energy for self diffusion

and kT - the product of Boltzmann constant and absolute temperature

This equation does not describe J correctly for an insulator where one can have $j = 0$. We suggest here to modify this empirical expression by replaing

$$\rho_e j \quad \text{by} \quad (C_2 + \rho_e j)$$

so that J does not go to zero for $j = 0$ (C_1 and C_2 are constants).

We propose here that this equation can be applied also to relevant effects along solid surfaces. Whereas the potential troughs in a solid are commonly used in connection with bulk diffusion, a corresponding trough system can be envisaged also for atoms physically adsorbed on solid surfaces, although they can be expected to exhibit smaller potential rims. The application of an electric field can now either be understood to distort the potential function such that the atoms have an increased probability to leave the well in those directions where the potential rims have been lowered due to the applied field. Or the electric field is taken to exert a force on partially or fully ionized atoms. These phenomena can be expressed by a replacement of Q by $Q + e\Delta V$ in eqn 1. On the other hand, the effect of an electronic wind would affect J by the electronic current j.

The ultimate aim is therefore here to establish whether these theoretical concepts are valid and then to determine the relevant parameters, for example by undertaking measurements at various temperatures so that Arrhenius diagrams can be constructed and Qand ΔV-values derived for the surface conditions of technological interest.

Here now a number of first measurement are reported concerning this subject of material transport as relevant for device life times.

IV.2 High Electric Fields Applied Between Closely-Spaced Lines on GaAs-Surfaces

In accordance with the proposed investigation appropriate test-samples have been prepared, suitable for studying lateral material transfer of metallic electrodes on planar GaAs structures.

The electrode systems shown in Fig. 11 consits of an inter-digitated narrow-finger Al structure, interconnected by two larger contact areas on each siede, and evaporated as thin films of 1000 - 2000 Å thickness onto a semi-insulating GaAs substrate of 300 µm thickness. The separation between adjacent finger electrodes equals in all cases the width of the metal electrode itself. In a first attempt this width was chosen to be 100 µm in order to avoid difficulties in preparing the long narrow-line structure by photolithography-techniques and to achieve between adjacent electrically intersected electrode edges reasonable high electrical lateral fields, in order to get detectable amounts of migrating material.

Whereas the structure shown in Fig. 11 is to be used to examine effects of lateral field diffusion, Fig. 12 shows a sample to be used for exploring effects of lateral temperature or electron-wind diffusion. The meander electrodes with the same spatial dimensions as described above are no longer alternately electrically intersected to each other, but switched in series. Thus no substantial electrical fields should occur at the electrode-substrate edges but a constant current. A realized sample of the first kind is shown by Fig. 13.

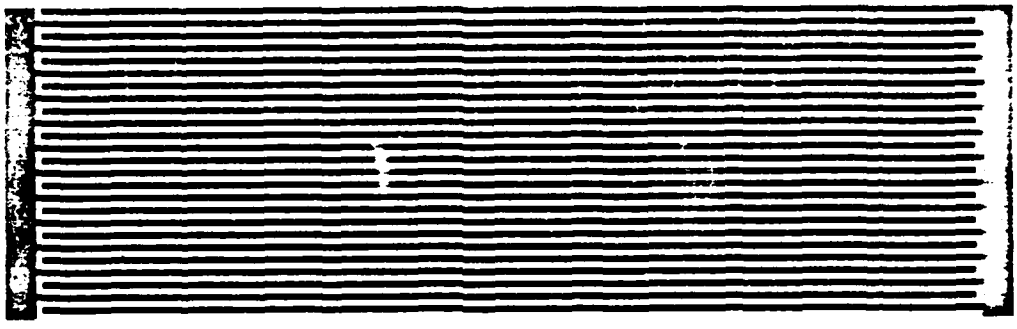

Fig. 11
Photomask of the interdigitated finger-structure

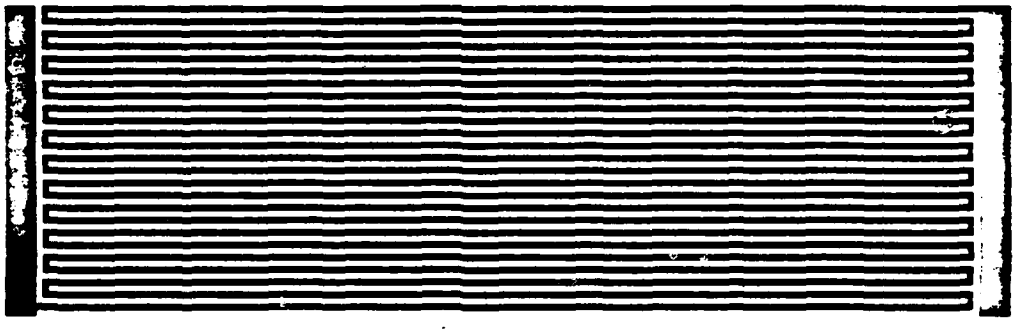

Fig. 12
Photomask of the meander structure

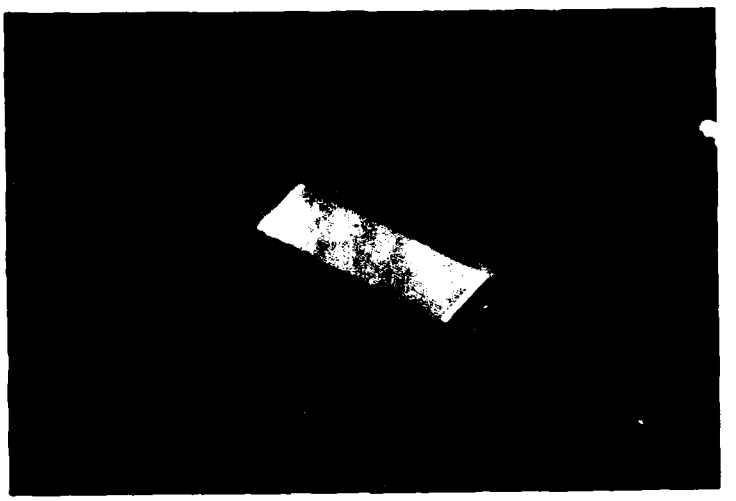

Fig. 13 Manufactured sample with integrated finger-electrodes

To accelerate long-time field induced failure mechanisms high fields of about 10^5 V/cm must be applied to the samples. Therefore a high-voltage micromanipulator test fixture was developed and built, in which the samples were contacted. This measurement set up is protected against ambient light to avoid a photocurrent in the GaAs substrate, which would decrease the breakdown voltage.

Applying high electric fields to the samples, the observed phenomena are very complex.

At first a distortion of the electrode edges by ionization of air could be observed. To investigate this effect separately, samples were produced by using a glass substrate. Whereas glass exhibits similarly good isolation properties as SiO_2, a typical isolator in GaAs-technology is perhaps less ideal. Fig. 14 shows the closely spaced Al-electrodes on glass before (a) and after (b) breakdown, which were photographed under a microscope. At both edges material is sputtered away. The measured I-V characteristics are in general agreement with the theory of gas discharge (Fig.15). In atmospheric air, cosmic and radio active radiation generate free charge carriers, which slowly recombine again[16].

Generation- and recombination rates are balanced so that a constant charge carrier density occurs. I a high field is applied between two electrodes, the charge carriers generated in the air are separated fast, and recombination does not take place.

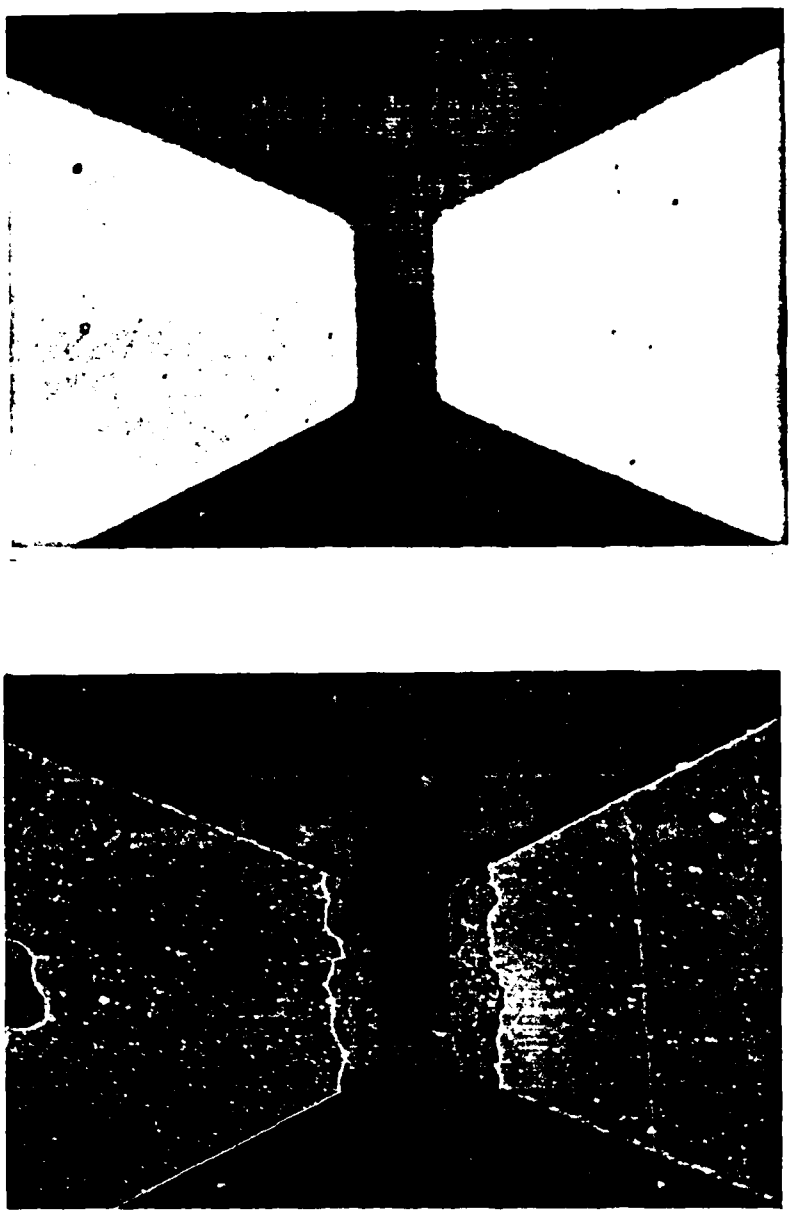

Fig. 14 Al electrodes on glass before (a) and after (b) breakdown

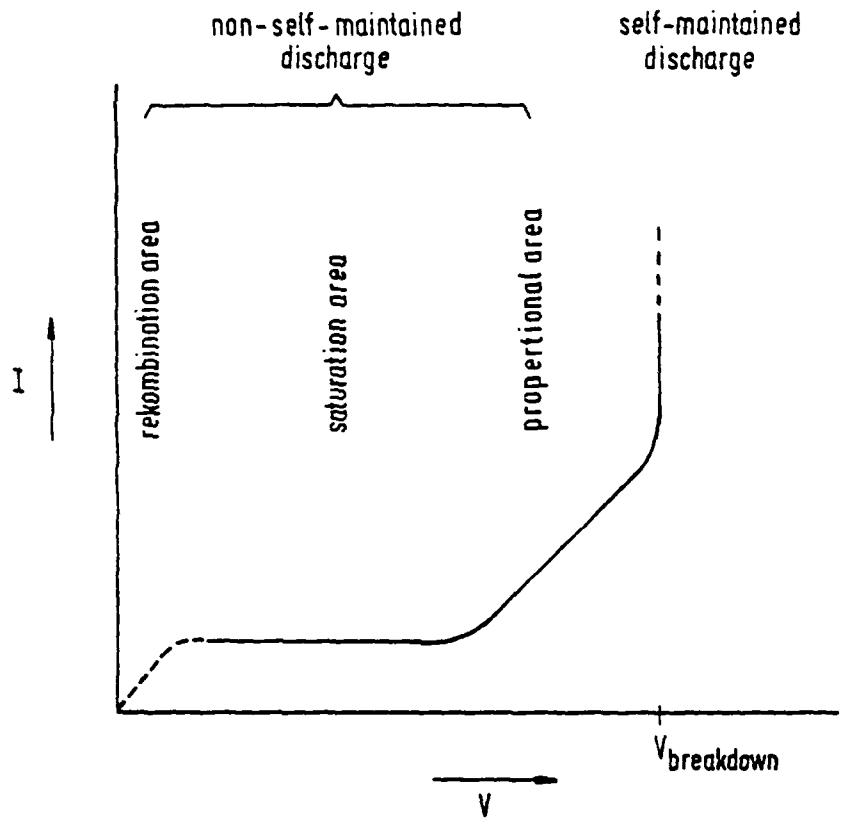

Fig.15 I/V characteristic of a gas discharge in atmosphere

Practically all the generated free charge carriers are transported to the electrodes and a saturation current flows which is proportional to the charge-carrier generation rate. If the voltage at the electrodes is further increased the current increases too. This growth occurs, when the charge carriers get such a high velocity in the electric field, that neutral gas atoms are ionised by impact. These generated secondary ions support charge carrier transport. The resulting ion bombardement destroyed the electrodes in the course of time. An instanteneous burnout takes place, when the just described non-self-maintained discharge pass into a self-maintained discharge. At this breakdown field strength the impact ionization leads to an avalanche-like increase of the free-charge-carrier number. Decisive to the amount of this breakdown field strength is besides the properties of the ambient gas (pressure, temperature) the electrode geometry. At an air pressure of 1 bar and a temperature of 20° C with Al-electrodes of a thickness of 1800 Å on glass, the breakdown field strength is measured. At an electrode distance of 10 to 15 µm a field strength of 2.6 to $2.8 \cdot 10^5$ V/cm has been obtained. On the other hand, for the same electrodes with a distance of 50 µm a value of 1.5 to $1.7 \cdot 10^5$ V/cm resulted. This dependence of the breakdown field strength upon the dimensions of the planar electrodes (thickness, length and distance between closely spaced electrodes) is investigated systematically at present.

To examine these destructive effects at long extended electrode lines, finger structures were produced on glass. Fig. 16 shows a photograph of such a device after a breakdown. This takes place at the edges of the electrode ends, where the electric field lines are condensed. At the sites where material is sputtered, new edges are formed, with a subsequent concentration of the field lines so that the destruction migrates along the electrode lines. This is documented by Fig. 16. At the lower cathode the destruction just started, whereas at the upper cathode the destortion is advanced. It is interesting here, that the destruction begins at the ends of the cathodes and not of the anodes. The explanation for this is that the positive free charge carriers consist of ionized atoms with the mass of the atomic cores, whereas the negative free charge consists essentially of free electrons. Consequently before the breakdown the bombardment damage of the cathode is more severe than that of the anode. The anode is affected subsequently primarly by material debris, which is sputtered out of the cathode and the bombards the anode.

If a high electric field is applied now to planar finger structures on s.i. GaAs, a lateral material migration between single fingers takes place additionally. Fig. 17 shows such a sample before (a) and after (b) a breakdown, and in a magnification (c) the migrated line material. For this migration of the line material, the basic processes of the energy exchange at interfaces are of particular significance.

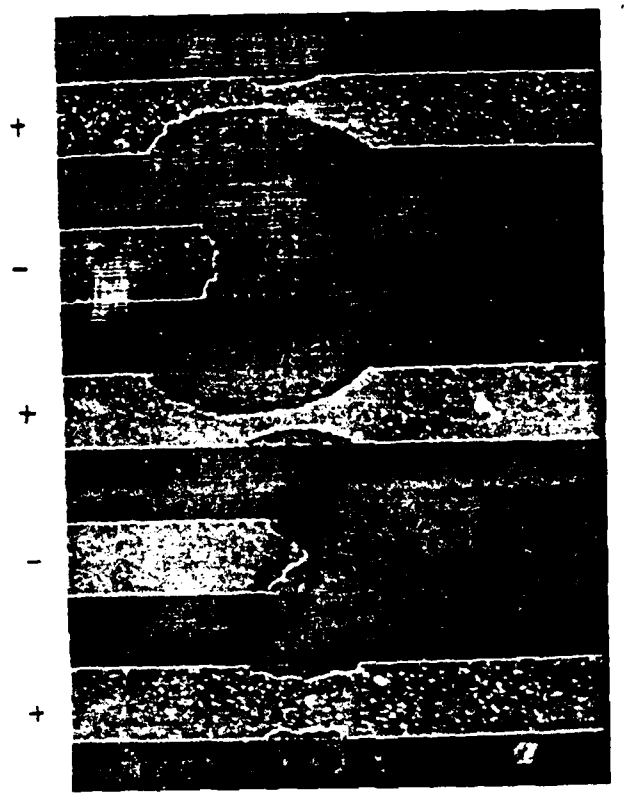

Fig. 16 Al fingers on glass destroyed by breakdown in air

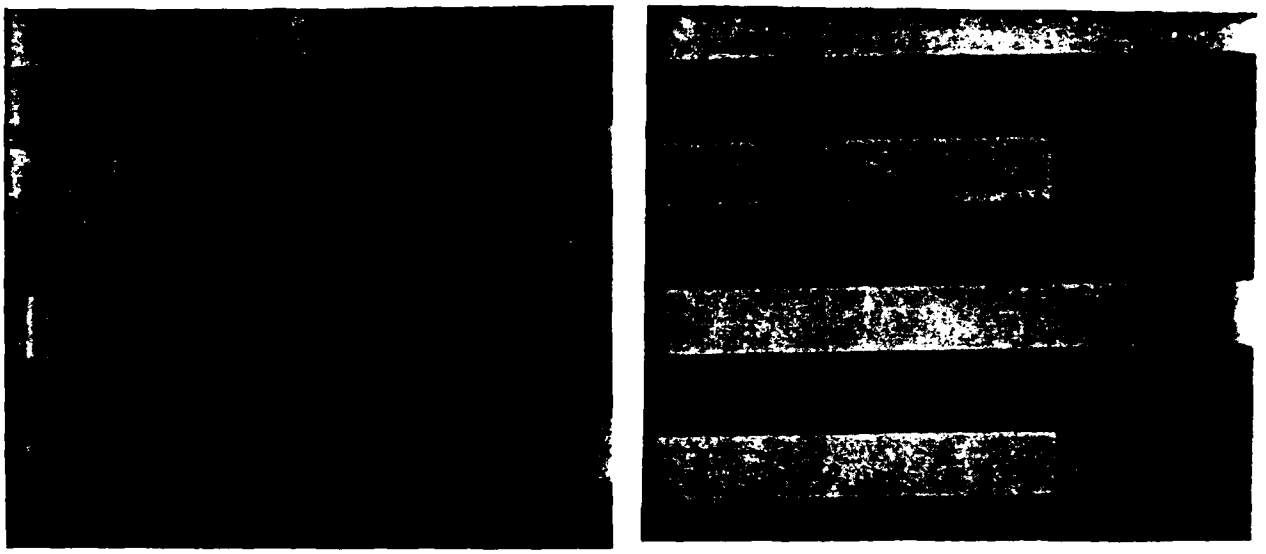

(a) 100 μm (b)

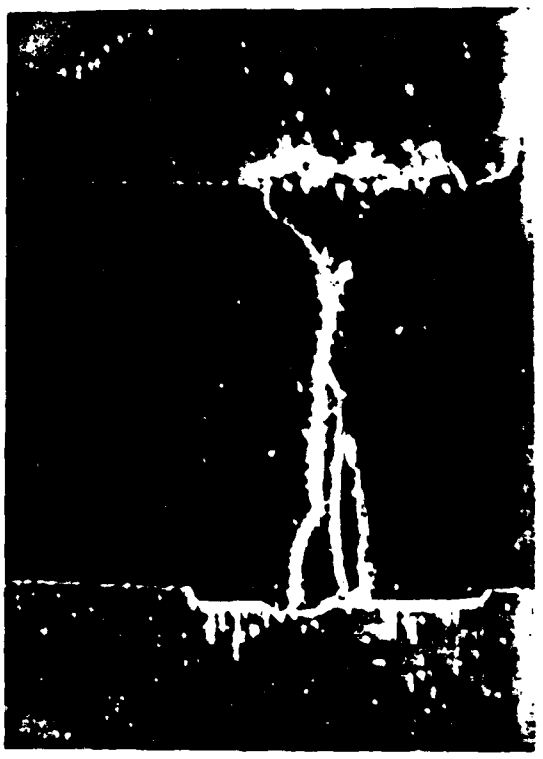

(c) 20 μm

Fig. 17 Breakdown between finger structures on semi-insulating GaAs
a - before breakdown; b - after breakdown; c - magnified breakdown of b

To describe these processes in greater detail than given in the introduction of this Chapter, and to propose here a possible model for material migration along free GaAs surfaces, an atom is considered which is positioned on the surface of a GaAs substrate. The atom is affected by homopolar (exchange-) forces with particular electron exchange or heteropolar (Coulomb-) forces with a full transition of the peripheral electrons to the electron shell of the substrate atom. A further approach of the atom to the substrate surface is prevented by the repulsive forces of the positive corecharges. For the substrate a two-dimensional surface potential field can be proposed[14]. In the simplest case of homogeneous atomic lattice this potential field is in both directions periodic (Fig. 18). A particle on the surface oscillates, depending on its kinetic energy, about a place, which is determined by a local energy minimum. It migrates on the surface if its energy surmounts the energy E_{ch} which is necessary for a site change. Normally the energy of the atom is not high enough to leave the force field of the surface atoms at once. If a high electric field is applied to the surface the function of the potential surface energy will be deformed in such a way that the energy, which is necessary for a site change, decreases (Fig. 18). A material migration takes place in the direction of the electric field.

If there is an atom on a substrate surface one obtains a further deformation of the function of the potential surface energy. That is the reason why in the immediate vicinity of an atom the energetic conditions cause preferred sites to exist next to that atom for

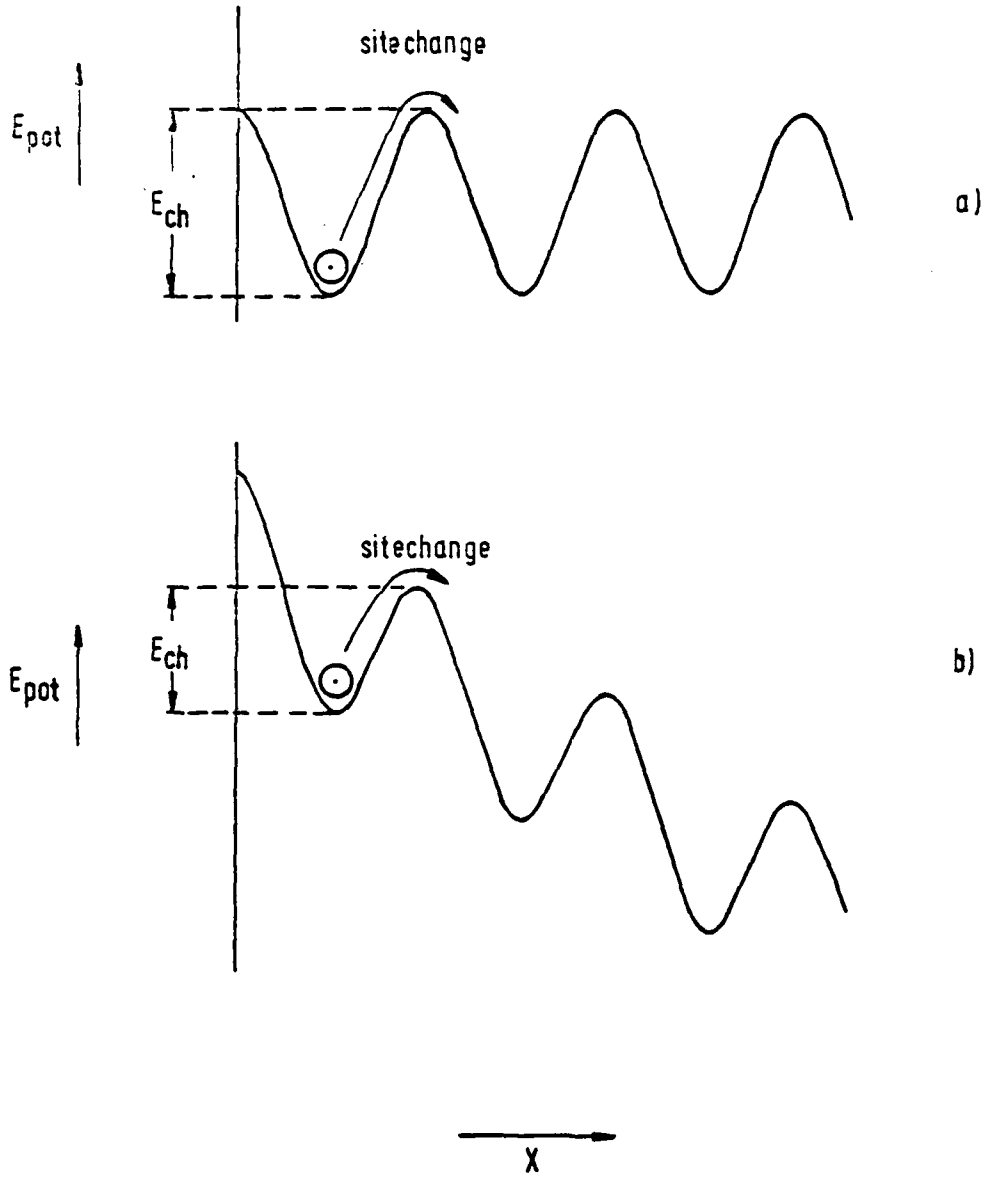

Fig.18 Model of site exchange process for metal atom at edge of metal finger structure (diagram of the potential energy for a homogeneous lattice of the surface atoms)
a - without externally applied electric field
b - with an electric field applied

further particles. Atoms which migrated along the surface or which originated from the electrode sputtering process across the surrounding atmosphere cause other atoms to follow preferantially. This explains the lateral whisker growth shown in Fig. 17 b and c. In the same way energetically preferred sites are formed by irregularities of the substrate surface like grain boundaries, dislocations e.t.c., along which material migrated already at a lower electric field.

Summarizing the results of the observed effects are as follows: The electric-field induced migration of electrode material from the anode to the cathode can be described by the deformation of the surface potential. According to the applied electric field the energy barrier for a site change of atoms has been decreased. Consequently the probability and with it the velocity of a lateral material diffusion increases with increasing electric field strength.

The growth of whiskers is explained by the energetically preferred sites in immediate vicinity of the already migrated material, similar to the material migration on irregularities of the substrate surface.

A clearly observed electric-field induced effect is in support of the proposed model of material migration by sputtered electrode particles. The destruction of the electrodes results from the bombardment of free charge carriers, which are accelerated in the electric field.

Important parameters of the effect of electric-field induced lateral material migration are the types of electrode- and substrate material, the properties of the ambient gas, the geometry of the electrodes and above all the treatment of the surface.

Our first experiments show therefore that s.i. GaAs-surfaces treated by some basic etchants need about double as high a field strength to induce lateral material transfer than non-treated samples. More precise investigations are planned so that the important features of the substrate surface will be clarified by using our surface analysis facilities (ESCA and ISS).

IV.3 Interdiffusion Across the Interface Metal-Semiconductor

The long-term stability of a metal contact on GaAs depends on any interdiffusive effects occuring by prolonged operation with high currents or voltages applied to that junction. In order to select initially a relatively simple me allization system commonly found with GaAs devices, we selected the problem of Al on GaAs and the application of a large electric voltage over a long time. The results found then would surely depend also on the compositional variation of the GaAs surface depending on the etch treatment of the GaAs wafer before metallization, the work undertaken so far, is to be fully combined with efforts such as those described in Chapter 2 above.

Analyses of failure modes, reducing the life times of semiconductor devices, show that metallizations on semiconductors are often more seriously affecting the reliability of devices than crystal defects[8]. With metallizations, the following failure modes can be distinguished:

1. Transport of metal along a current-carrying conductor due to the impulses provided by drifting electrons - the so-called electron-wind effect. We are not yet addressing ourselves to this effect as stated above.

2. Transport of metal atoms into the semiconductor.

3. Transport of semiconductor atoms into the metal film [9,11] and

4. Diffusion of atoms from the atmosphere into the metal and semiconductor [10].

Since metallization failures are mostly long-term effects [2,6], examinations in this field require accelerated experiments in order to observe these phenomena within suitable times. Therefore, either the electrical field strength or the temperature or both are increased as compared with normal operational conditions.

Here then, we studied the influence of high electrical fields, the interdiffusion at an Al-GaAs interface. The investigations have been carried out by also making use of microscopy and by measurements in our Leybold-Heraeus XPS facility.

As reported from accelerated life tests [9], interdiffusion at the gate-GaAs interface is the common failure mode of GaAs-FETs. Investigations of the Al-GaAs interface indicate that interdiffusion between aluminum and GaAs occurs even at the usual operating temperatures of GaAs-FET-devices [9]. Reliability tests reveal that these effects are also bias sensitive [11]. Expecially with regard to the reliability of GaAs-FETs, it therefore seems to be very interesting to obtain more detailed information of these

interdiffusion phenomena. In accordance with the application to ERO, we started this interdiffusion work using semiinsulating GaAs and aluminum and applied a high electrical field over periods of days and weeks.

Semiinsulating GaAs was selected because this material permits obtaining high electrical field strengths while the current flow in the sample remains negligeable. By these means we are able to exclude thermal- und current enhanced interdiffusion.

In order to detect any interdiffusion effects at the aluminum-GaAs interface that can be related to an electrical field, two identically prepared samples were fabricated initially. One has been exposed to an electrical field for many days, whereas the other one only served as a reference sample without being treated electrically in any way. The electrical field has always been applied between the metallized front and backsides of the sample (see Fig. 19). Afterwards an XPS sputter-profile measurement of both samples has been performed in our Leybold-Heraeus XPS-facility. Comparing these sputter profiles leads to the results, described below.

Figures 20 a and b show the structure of the test samples. The semiinsulating GaAs used was supplied by Wacker Chemitronic. It had a (100) surface orientation and was polished on one side. First the wafer was cleaved into several samples (their size was about 6 . 4 mm^2), then the samples were boiled in acetone,

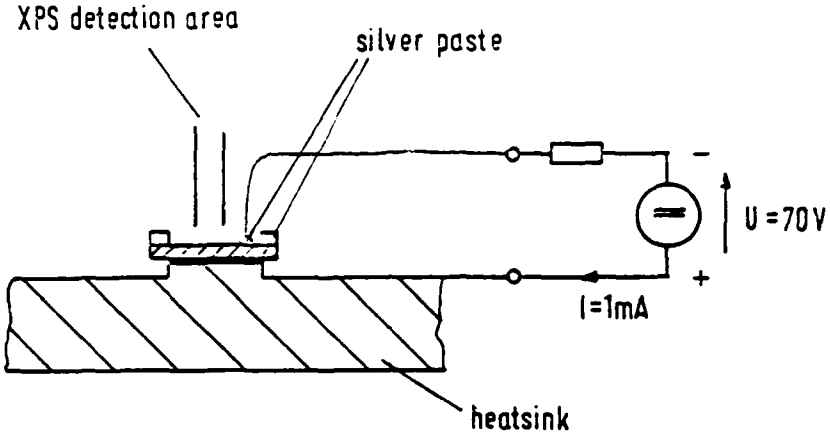

Fig. 19 Mounting of the sample, experimental details

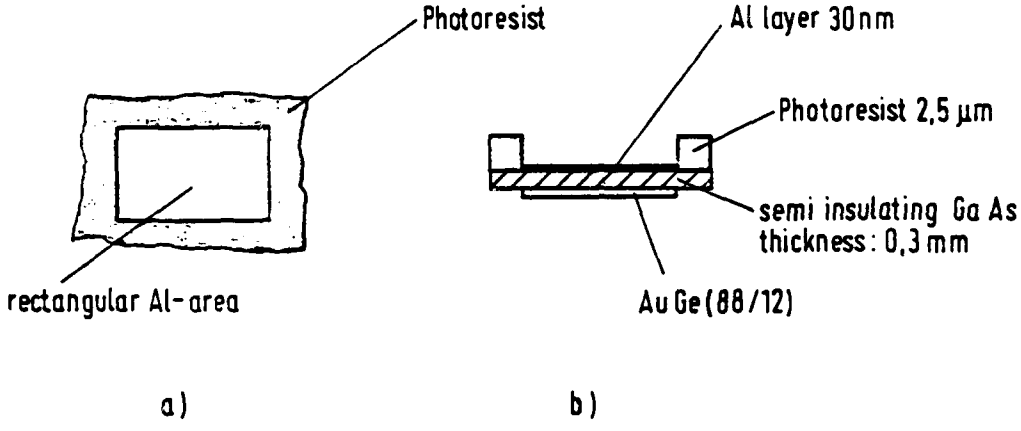

Fig. 20 a) - Top view of the prepared samples
b) - Cross-section of the samples

trichlorethylen and methanol to remove organic contaminants. After etching in NaOH + H_2O_2 for 20 seconds (1/1 mixture of 2 % per weight NaOH and 1,2 % per volume H_2O_2 in H_2O; etching rate 100 Å/min [3]) a rectangular area of AuGe (88/12) was evaporated onto the umpolished side of the samples and annealed at 450° C in flowing nitrogen for 5 min. The polished sides of the samples were etched by NaOH + H_2O_2 because relatively high avalanche breakdown voltages had been obtained with it in comparison with many other etchants [11]. The GaAs surface was then covered with a rectangular, 30 nm thick aluminum film. To obtain an almost identical metallization of the samples they were mounted side by side in the evaporator. A rectangular metallization structure was chosen firstly to achieve a defined detection area for sputter-profiling, and secondly to avoid an undefined field-strength distribution along the corners of the sample during electrical treatment. An area of 3 x 5 mm has been found sufficient to achieve a suitable XPS sensitivity. Moreover the contacts for electrical treatment can then be placed outside the detection area of our XPS facility (about 1 . 10 mm^2) and can therefore not cause any error in measurement (see Fig. 19). The relatively thin aluminum film allows sputter profiling in not too long times. The area between the metallization on the polished side of the sample and the sample edges is covered with photoresist (2,5 µm, hardened at 80° C for two hours). To prevent detecting Ga and As that is not located in the defined rectangular area. The photoresist is an organic compound producing an XPS spectrum which does not disturb the intended sputter-profile-measurement.

During electrical treatment the sample was driven near the avalanche breakdown to achieve the highest possible field strengths. A voltage of 70 V (current 1 mA, polarity corresponding to Fig. 19) was applied for many days. The sample was mounted on a heatsink with silver paste. Calculations, taking into account the thermal conductance of GaAs [12] reveals that thermal effects at the operating conditions described above can be neglected. The aluminium structure on the polished side of the sample was contacted by a thin wire, also fixed with silver paste. It is to be pointed out that the results presented below are confirmed by more than one test set of samples.

Fig. 21 shows the XPS sputter profile of a reference sample, whereas Fig. 22 indicates the XPS sputter-profile of a corresponding sample that had been treated electrically for 182 hours. The amplitudes of the O $1s_{1/2}$; As $2p_{3/2}$; Ga $2p_{3/2}$ and Al $2p_{1/2}$ n.ox. (non oxidized) count rates are normalized on the corresponding maximum peak value occurring in the sputter profile. The count rates of oxidized aluminum (al $2p_{1/2}$ ox.) is normalized on the maximum value of the non oxidized Al $2p_{1/2}$ peak to estimate the relation between oxidized and non oxidized aluminum.

In Figures 23 and 24 the corresponding O, As, Ga and Al lines of the reference sample and the electrically treated sample at different sputter times are compared.

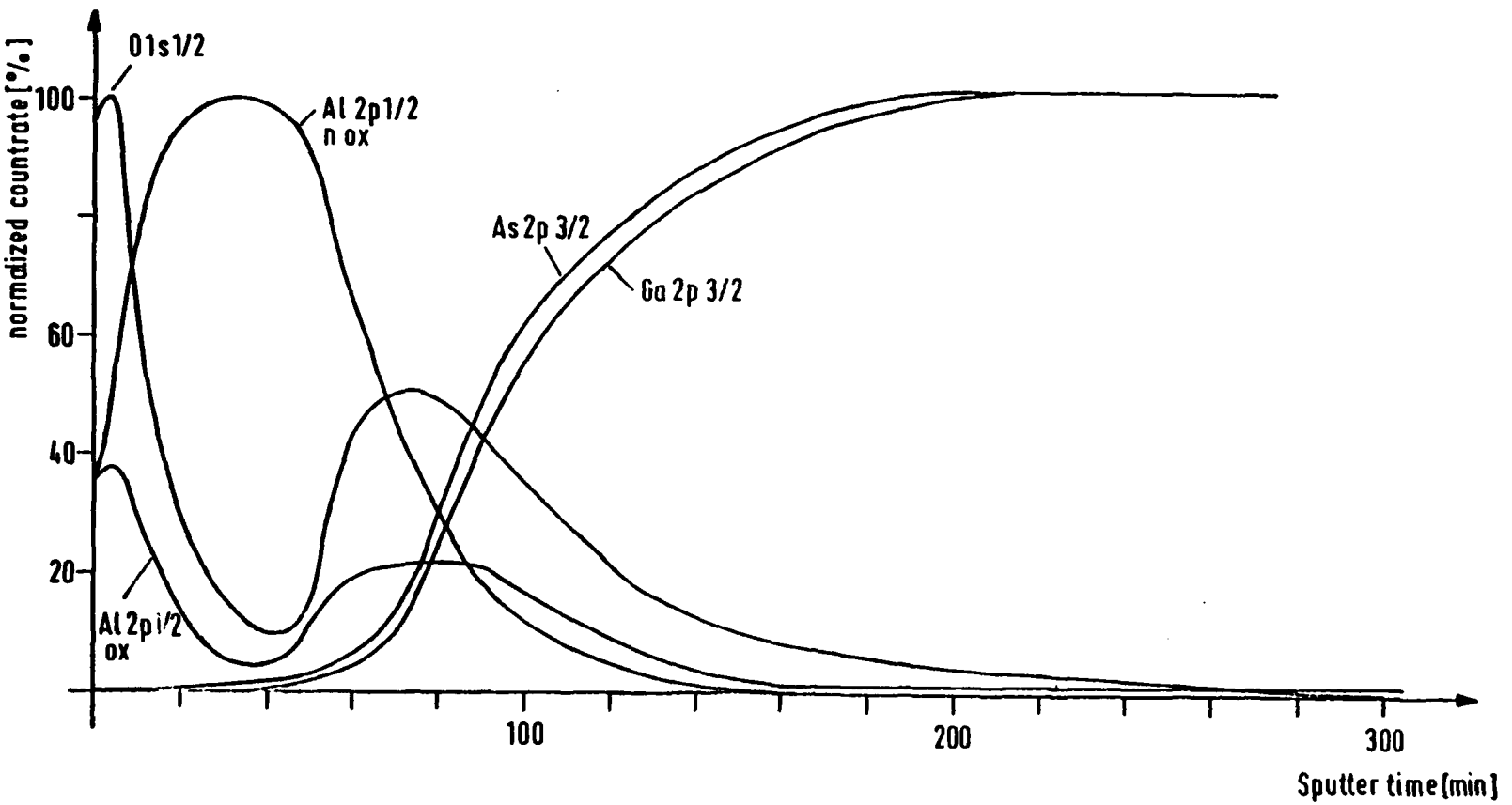

Fig. 21 Sample without applied electric field

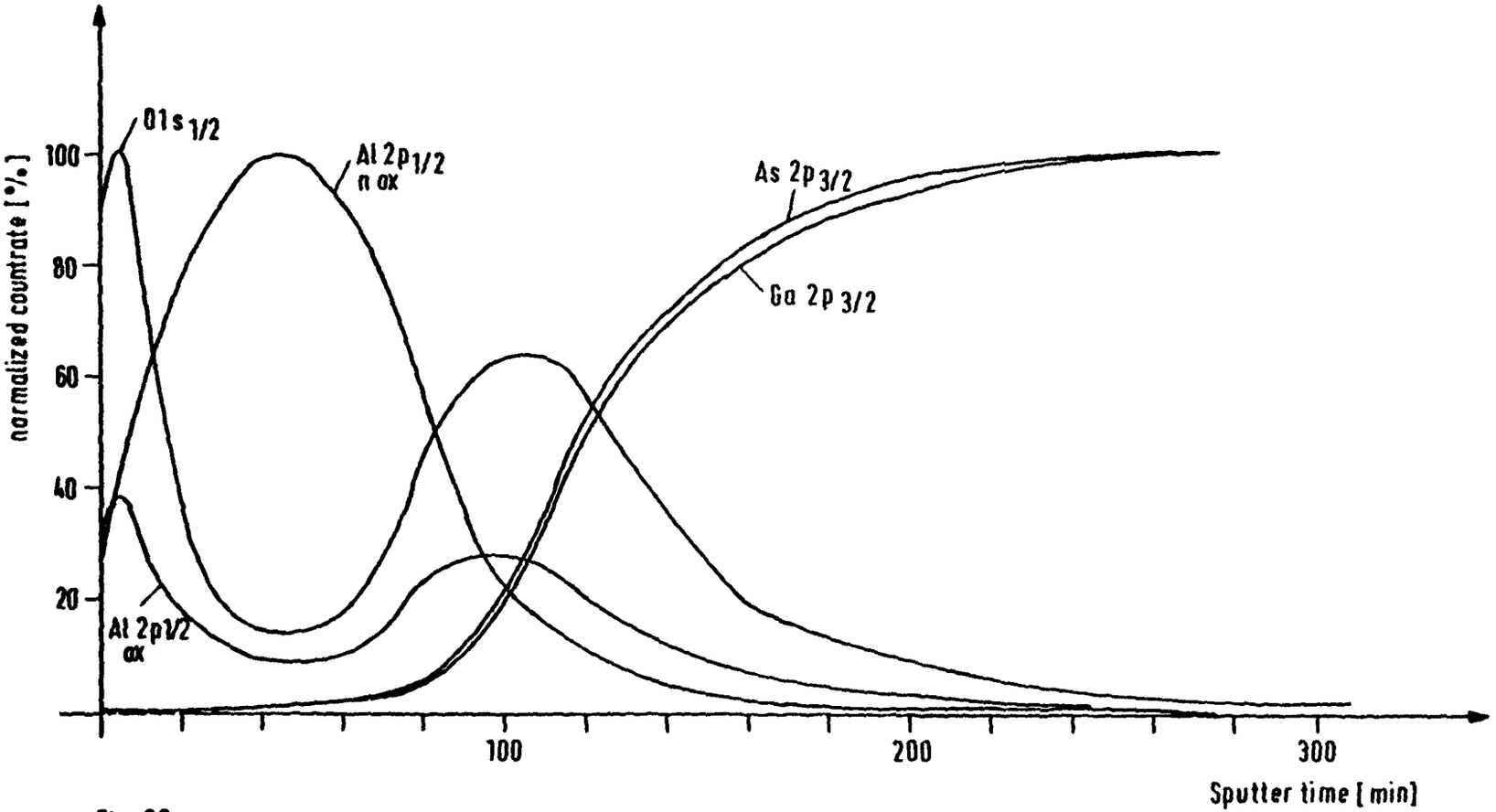

Fig. 22 Sample which has been driven near the avalanche breakdown for 185 hours

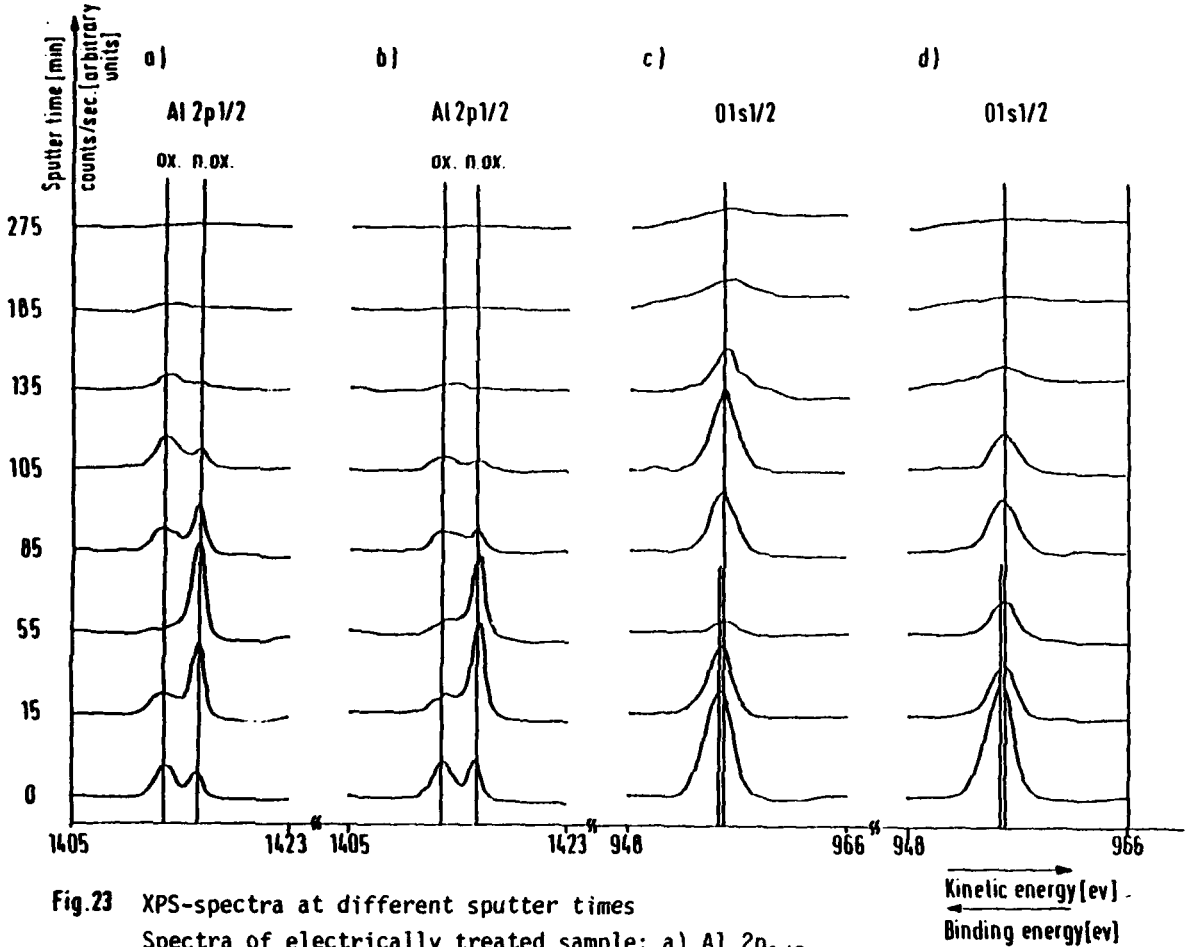

Fig.23 XPS-spectra at different sputter times
Spectra of electrically treated sample: a) Al $2p_{1/2}$
c) O $1s_{1/2}$
Spectra of corresponding reference sample: b) Al $2p_{1/2}$
d) O $1s_{1/2}$

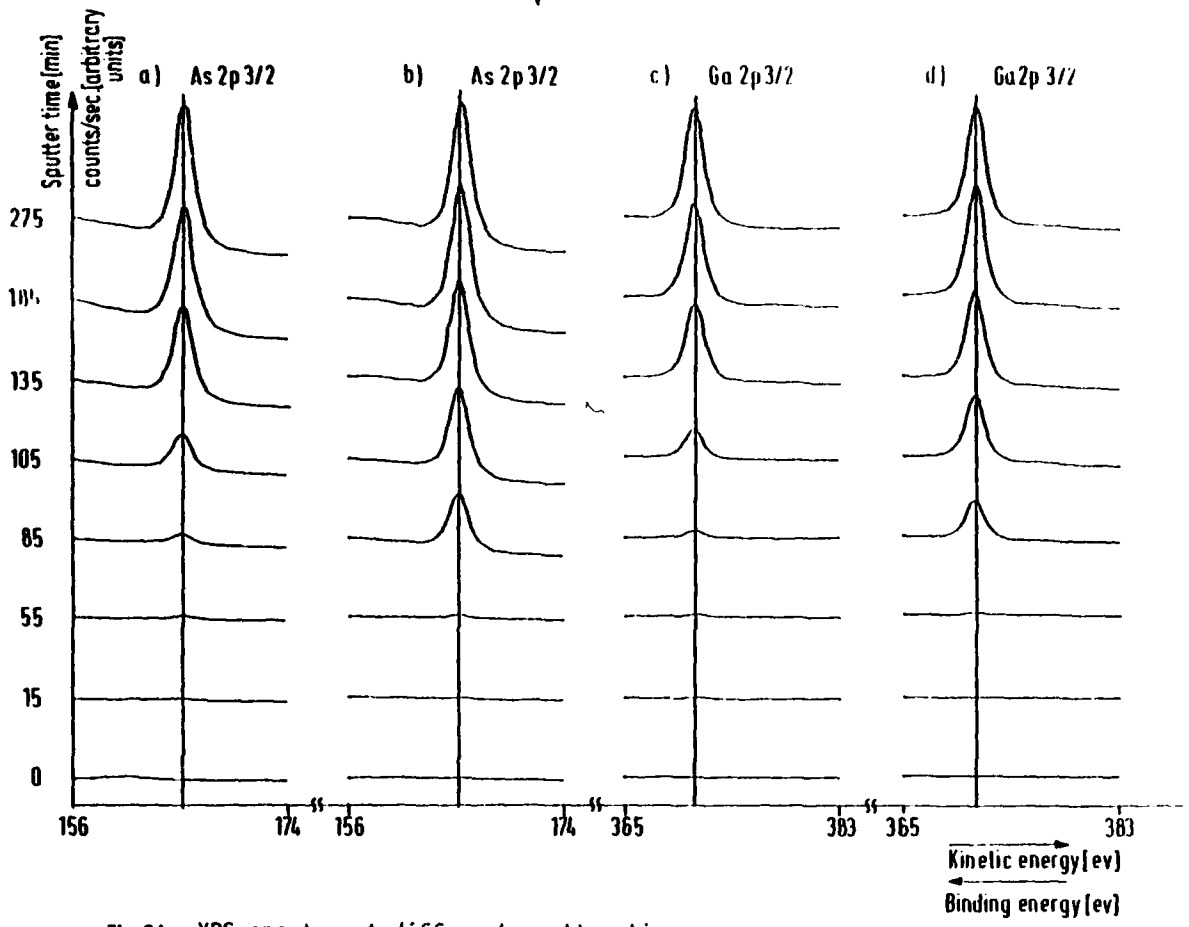

Fig.24 XPS-spectra at different sputter times

Spectra of electrically treated sample: a) As $2p_{3/2}$
c) Ga $2p_{3/2}$

Spectra of corresponding reference sample: b) As $2p_{3/2}$
d) Ga $2p_{3/2}$

Analyzing the sputter profiles and the XPS spectra one can suggest several general points due to the electrical treatment of the sample.

1. The curve of the non oxidized aluminum (Al $2p_{1/2}$ n.ox.) has broadened after electrical treatment. At the first sight one might interpret this behaviour incorrectly as a diffusion of aluminum into GaAs. In this case, however, the ratio of the Al to Ga or As concentration should increase, and the slope of the concentration curves at the interface should decrease in comparison with the corresponding concentration curves in Fig. 21 where no external electric field was applied. Since none of such observations were made with Fig. 22 it seems to be unlikely that an aluminum diffusion into GaAs had occured. The broadening of the concentration curve is, however, likely to be a consequence of a structural change in the aluminum layer during the electrical treatment, resulting finally in a decreased ion-etching rate. This structural change can perhaps also be referred to in connection with different grain sizes and grain boundaries in the Al film due to a field enhanced diffusion of charged lattice defects into lattice vacancies [13] as described more fully below.

2. Comparing the shape of the O $1s_{1/2}$ curves in Figures 21 and 22 one finds an increased oxygen amount at the interface in Fig. 22. This can be the consequence of an oxygen indiffusion from the

ambient but it can also be due to a thicker layer of native oxide on the GaAs surface before the evaporation of the aluminum film. Further experiments have to be undertaken to clarify this behaviour. Nevertheless it is interesting that the oxygen at the interface is entirely bonded to the aluminum whereas Ga and As is not oxidized (see Figures 23 and 24). Besides that, the chemical bonding between aluminum and oxygen seems to be different from the bonding at the surface of the Al layer. This is indicated by different curvatures of the Al $2p_{1/2}$ line at the surface or at the interface (Fig. 23 a and b).

The increase of the proportion between the O $1s_{1/2}$ and the Al $2p_{1/2}$ (ox.) lines at the Al surface can perhaps be referred to a physical adsorption of oxygen at the aluminum surface. This statement is supported by a corresponding shift of the O $1s_{1/2}$ line at the Al surface (Fig. 23 c and d).

3. The slope of the Ga $2p_{1/2}$ and Al $2p_{1/2}$ curve in the range between 70 and 90 min sputter time in Fig. 22 has decreased compared with the corresponding slope of these curves in Fig. 21 (again range 50 ... 70 min sputter time). This seems to be explained as a diffusion of As and Ga into aluminum across the interface. Moreover, the proportion between Ga and As in this area has become more stoichiometric after the electrical treatment, which can perhaps be explained by an outdiffusion of As through the thin Al film and a subsequent evaporation from the Al surface since no significant amount of As has been detected there.

IV.4 Mechanisms of Field-Enhanced Interdiffusion

In the literature two different mechanisms of field enhanced interdiffusion are presented [8]. In both mechanisms the existence of lattice vacancies is required. Neighbouring atoms or ions are able to jump into these vacancies if the electrical field can support sufficient energy for this jump by one of the two mechanisms. The first mechanism requires ions in the neighbourhood of the vacancies that can be pulled by the electrical field and jump into the vacancy. The second mechanism depends on an electron flow that transfers its impulse to lattice atoms and can therefore increase the probability of atoms in the neighbourhood of vacancies to change places with them.

It can be expected that the second effect will not be the dominant mechanism in our experiments reported in 4.3 since the current density used is much smaller than in investigations of other authors dealing with electron-impulse-transfer stimulated material diffusion [8].

The observed diffusion of As and Ga into aluminum at the interface and perhaps the structural change in the aluminum layer during electrical treatment is then to be explained by the first mechanism. This assumes the existence of positively charged Al ions in the Al-film and positively charged Ga and As ions at the interface. Positive ions move in the direction of the electrical field by changing places with vacancies which therefore move in the opposite

direction. This means that in our experiment only Ga and As is diffusing into the Al layer, and no Al into the GaAs.

It has been shown in [8] that at temperatures beyond 400° K grain boundaries are preferred diffusion paths in metals and that a field enhanced diffusion along grain boundaries can fill up voids in the metal and can change grain sizes. This might be a mechanism, explaining our observed structural change in the Al layer.

In summary, the results of Chapter 4.3 have shown field enhanced interdiffusion effects at the Al-GaAs interface. Our first experiments have been carried out on semiinsulating GaAs, to prevent effects related on a current flow. An XPS sputter profiling measurement shows the chemical compositions of the Al-GaAs interface in dependence on the sample treatment.

Our results indicate a diffusion of As and Ga into aluminum and a structural change in the Al-layer after prolonged electrical treatment. It seems that the observed effects can be explained by corresponding theories of Wever or Huntington[13].

In the future, this effort is to be extended. It is in particular envisaged to look for a correlation between interdiffusion effects and the electrical behaviour of the samples.

CHAPTER V

Conclusion and Recommendations

GaAs-wafer surfaces have been analyzed by XPS and ISS after various typical device-manufacturing-technology steps were applied. A surprising difference in the chemical composition of Ga, As and their oxides was found for such common agents as deionized water, basic or acidic etchants, etchants based on reaction-limited or diffusion-limited processes, with or without prior sputter etching, etc. It seems that methanol produces only small modifications to the GaAs surface. Evidence was found for chemically and physically adsorbed oxygen.

ISS gives information about the surface monolayer and therefore information about a normally available but quickly ion-bombardment-removable dirt layer and many other directly surface-atomic-layer oriented effects. In order to avoid the difficulties of measurement errors by long ion etch times changing the analyzed composition by selective ion etching effects, the studies were undertaken by the various 2p and 3d emissions since they originate from different escape depths. In this way some limited amount of relatively reliable depth dependent information can be obtained near the surface.

The physical processes in connection with the instability of metal film structures on GaAs have been studied. In connection with the initiation of short-circuiting channel formation between neighbouring metal electrodes it was established that ionizing high-field breakdown of the atmosphere over the electrode structure

causes sputtering at the negatively biased electrode first, with film removal at the electrode edge and metal deposition also near the positively biased electrode edge. There material migration is then initiated in accordance with the theoretical concepts of potential-well distortion by externally applied electric fields and by any atom trapped by such a well, i.e. by physical adsorption of, for example, the sputtered cathode-edge material.

The effects of a high applied electric field are complex but can be understood as a field-assisted diffusion of Ga and particularly As in Al, and of Al into the vacancies and grain boundaries of the Al-film thus leading to a denser Al layer. There are oxidizing processes with the high fields due to both the original native oxide on GaAs as well as probably also in-diffused oxygen, both in the Al film as well at the interface with the semiconductor.

The concepts associated with light emission have been clarified. They are based on avalanching processes which are affected indirectly by the surface conditions of the GaAs wafer since the current-flow crowding at metal edges and other metal-semiconductor interface irregularities are modified by the chemical composition. Here further information can be obtained from the recently completed doctoral thesis of one of the authors of this report (E. Huber[11]).

It can therefore be concluded that the studies of the first year of this project have already resulted in useful information regarding the physical processes associated with the operational conditions typical for life-time limitations. These results also

clearly help to define the most profitable orientation this work should have in the future.

In particular, it is now recommended to study also other material-bridge forming effects between neighbouring electrodes, as partly seen already by one of the authors in related studies during his sabbatical work[15]. This effort is then to be performed together with the various technology processes for which the chemical data has also been presented in this report. The aim is to undertake this investigation as a function of ambient temperature so that the relevant Arrhenius plots thus made can give the relevant activation energies. Of course the chemical surface-layer information can always be established then with our surface-analytical facilities.

Similarly, the field-assisted material transport, associated with thin metal films on GaAs, is to be studied also for different polarities of applied voltage, for the various technological surface conditions studied so far and for some of the other metal systems commonly used for GaAs devices. Here is the aim too, to establish if possible the data for various ambient temperatures to obtain the relevant activation energies from Arrhenius plots.

Finally, efforts are to be started soon to evaluate the phenomena of material transport associated with the "electron wind". This is particularly relevant for current transport along such narrow structures as the gate electrode on MESFETs.

APPENDIX

List of Student Projects related to the Present Report

1. F. Krizek, S. Sihombing - St 1196 - 19.07.1982
   Galvanische Abscheidung und elektrische Untersuchungen von Goldkontakten auf GaAs
   (Here in particular the ideality constant n and the saturation current is investigated for various etchants)

2. R. Israel - D 1202 - 16.05.1982
   Beeinflussung der Durchbruchstrahlung von GaAs Schottky Dioden durch Oberflächenpassivierung mit Eigenoxid
   (It is found that light emission is maximal for a native oxide of 800 Å thickness)

3. S. Sihombing - D 1248 - 16.02.1983
   Untersuchung des Einflusses der Oxiddicke und des Kontaktmetalls auf die Durchbruchstrahlung von GaAs MOS Dioden mit dünnem Oxid
   (A systematic evaluation of light emission for HCl and NaOH-type etchants)

4. F. Krizek - D 1251 - 02.03.83
   Optische Bestimmung der Barrierenhöhe von Schottkydioden auf unterschiedlich geätzten GaAs Oberflächen
   (It is found that the barrier height for NaOH-type etching is around 0.95 eV, whereas that with HCl-type etchants is about 1.0 eV)

5. M. Portugall - D 1259 - 05.04.83

Untersuchung von lichtemittierenden GaAs Schottkydioden bei tiefen Temperaturen

(Here, among other data it was found that the saturation current is higher for NaOH etched surface than for HCl etched ones)

6. A.L. Setiawan - D 1263 - 02.05.83

Untersuchung des Lawinendurchbruchs zwischen eng benachbarten Kontakten auf semiisolierendem GaAs

(Breakdown effects were studied between two coplanar metal electrodes on GaAs)

7. A. Charzakas - D 1308 - 12.03.84

Experimentelle Untersuchung des Verhaltens unterschiedlich gestalteter Metall-Halbleiter-Übergänge bei hohen elektrischen Feldstärken

(Experimental investigation of variously aged metal-semiconductor transitions for high electric fields)

8. N. Grigoriadis - D 1303 - 28.02.84

Untersuchung der Spannungsfestigkeit eng benachbarter Elektroden für monolithisch integrierte HF-Schaltkreise

(Voltage stability of closely spaced electrodes of monolitically integrated microwave circuits)

9. G. Pitz - St 1292 -

Materialwanderung zwischen eng benachbarten Elektroden auf semiisolierendem GaAs

(Material migration between two closely spaced electrodes on semi-insulating GaAs)

10. H. El-Hage - D 1289 - 09.01.84

Untersuchung von Schottkydioden auf gesputterten GaAs-Oberflächen

(Schottkydiodes on sputter-etched GaAs surfaces)

11. W. Graßmann - St 1284 -

Herstellung von Mikrostrukturen für Feldeffekttransistoren auf GaAs und InP

(Microstructuring for field-effect transistors on GaAs and InP)

12. U. Harich - D 1283 - 09.09.83

Studie zur Rechnersimulation ohmscher Kontakte auf InP mittels eines Tischcomputers

(Computer-simulation of ohmic contacts on InP using a desk calculator)

13. A. Koppe - D 1275 - 01.08.83

Herstellung ohmscher Kontakte auf InP durch elektrolytische Abscheidung von Zn

(Production of ohmic contacts on InP by electrolytic deposition of Zn)

14. F. Hartmann - D 1274 - 25.07.83

Der Einfluß der Strombelastung auf die Strom-Spannungs-Kennlinien von GaAs-Schottky-Dioden

(The effect of the applied current on the I/V characteristics of GaAs Schottky diodes)

Doctoral Thesis completed in the course of the reported year:

E. Huber - D 17 - 22.12.83

Untersuchung der Lichtemission beim Lawinendurchbruch von GaAs-Schottkydioden

List of Illustrations

Fig. 4 XPS-spectra

row 1 identical with Fig. 3 row 6

row 2 after reoxidation in air for 30 min

row 3 after short ion-etching

row 4 after heavy Ar^+ etching similar to that before spectrum given by Fig. 3 row 6

Fig. 5 Curve-fitted experimental spectrum of the As 3d - orbital of Fig. 3 row 6

Fig. 6 ^{4}He-ISS aquivalent to XPS of Fig. 4 row 2

Fig. 7 ^{4}He-ISS spectra

row 1 aquivalent to XPS of Fig. 3 row 1

row 2 aquivalent to XPS of Fig. 3 row 3

row 3 aquivalent to XPS of Fig. 3 row 6

Fig. 8 ^{20}Ne-ISS spectra

row 2 aquivalent to XPS of Fig. 3 row 2

row 3 aquivalent to XPS of Fig. 3 row 3

row 4 aquivalent to XPS of Fig. 3 row 4

row 5 aquivalent to XPS of Fig. 3 row 5

row 6 aquivalent to XPS of Fig. 3 row 6

Fig. 9 Depth profile of Ga and As by detailed ^{20}Ne-ISS analysis

Ga|GaAs| : concentration of Ga in GaAs-compound

As|GaAs| : concentration of As in GaAs-compound

Ga : concentration of Ga after the given etch step

As : concentration of As after the given etch step

Fig.10 Reverse I-V characteristics of GaAs Schottky barrier diodes of different doping concentrations

(a) $n = 2 \cdot 10^{16}\ cm^{-3}$

(b) $n = 4.7 \cdot 10^{17}\ cm^{-3}$

(c) $n = 1 \cdot 10^{18}\ cm^{-3}$

The solid lines are calculated tunneling currents for the following doping concentrations

(a) $n = 2 \cdot 10^{16}\ cm^{-3}$

(b) $n = 3.5 \cdot 10^{17}\ cm^{-3}$

(c) $n = 1.5 \cdot 10^{18}\ cm^{-3}$

Fig.11 Photomask of the interdigitated finger-structure

Fig.12 Photomask of the meander structure

Fig.13 Manufactured sample with interdigitated finger-electrodes

Fig.14 Al electrodes on glass before (a) and after (b) breakdown

Fig.15 I/V characteristic of a gas discharge in athmosphere

Fig.16 Al fingers on glass destroyed by breakdown in air

Fig.17 Breakdown between finger structures on semi-insulating GaAs

a - before breakdown

b - after breakdown

c - magnified breakdown of b

Fig.18 Model of site exchange process for metal atom at edge of metal finger structure, (diagram of the potential energy for a homogeneous lattice of surface atoms)

a - without externally applied electric field

b - with an electric field applied

Fig.19 Mounting of the sample, experimental details

Fig.20 a - top view of the prepared samples

b - cross-section of the samples

Fig.21 Sample without applied electric field

Fig.22 Sample which has been driven near the avalanche breakdown for 185 hours

Fig.23 XPS-spectra at different sputter times

Spectra of electrically treated sample: a) Al $2p_{1/2}$

c) O $1s_{1/2}$

Spectra of corresponding reference sample: b) Al $2p_{1/2}$

d) O $1s_{1/2}$

Fig. 24 XPS-spectra at different sputter times

Spectra of electrically treated sample: a) As $2p_{3/2}$
c) Ga $2p_{3/2}$

Spectra of corresponding reference sample: b) As $2p_{3/2}$
d) Ga $2p_{3/2}$

References

|1| J.C. Irvin, A. Loya: Failure
Mechanisms and Reliability of Low-Noise GaAs FETs
Bell Syst. Techn. J. 57, 1978, p 2823

|2| H. Adachi, H.L. Hartnagel
GaAs Schottky Light Emitters for the Study of Surface
Avalanching and Electroluminescence
J. Vac. Sci. Technol., 19, 1981, p 427

|3| S.H. Wemple et al
Long-Term and Instantaneous Burnout in GaAs Power FET's:
Mechanisms and Solutions
IEEE Trans. Electron Devices, 28, No 7, 1981, p 834

|4| H. Adachi, H.L. Hartnagel
Experimental Data on Light Emission Behaviour from GaAs
Schottky Contacts
Int. J. Electronics, 52, 1982, p 89

|5| W. Ranke et al
Orientation Dependence of Oxygen Absorption on a Calindrical
GaAs Sample
Surface Science, 122, 1982, p 256

|6| M.J. Howes, D.V. Morgan (ed.)
Reliability and Degradation - Semiconductor Devices and
Circuits
J. Wiley & Sons, Chichester, N.Y. Brisbane, Toronto, 1981

| 7| W. Fallmann, H.L. Hartnagel
Metallic Channels Formed by High Surface Fields on GaAs Planar Devices
Electronics Letters, Vol 7, No 23, 1971, pp 692-693

| 8| J. Hersener, T. Ricker
Elektrotransport in Aluminium Leiterbahnen
Wiss. Ber. AEG-Telefunken, 48, 1975, Issues 2,3, p. 46

| 9| W. Anderson, A. Christou and J.E. Davey
Amorphous Thin Film Diffusion Barriers on GaAs and InP
Thin Solid Films, Vol 104, 1983, pp 57-67

|10| C.-A. Chang
Similarity in Interactions Between Metal-Semiconductor and Metal-Metal Interfaces
J. Vac. Sci. Technol., 21(2) July/Aug. 1982, pp 639-642

|11| E. Huber
Untersuchung der Lichtemission beim Lawinendurchbruch von GaAs Schottkydioden
Dissertation, Technische Hochschule Darmstadt, 1983

|12| W. Fallmann, H.L. Hartnagel, P.C. Mathur
Experiments on Heat Sinking of Semiconductor Devices
Electronics Letters, Vol 7, 1981, p 512-513

|13| H. Wever
Elektro- und Thermotransport in Metallen
Barth Verlag, Leipzig, 1973

|14| E. Phillippow
Taschenbuch Elektrotechnik
VEB Verlag Technik, Berlin, 1978, Band 3, p. 130-135

|15| J. Dell, T.S. Kalkur, Z. Meglicki, A.G. Nassibian, H.L. Hartnagel
Au-Ge-Ni Migration Affected by Operating Conditions of GaAs FETs
Sol. State Electronics, to appear in 1984

|16| C. Gerthsen, H.O. Kneser, H. Vogel
Physik
Springer Verlag, Berlin/Heidelberg/N.Y., 1977, p 3o5-327

END

DATE
FILMED

4 84

DTIC